REMARKS

Favorable reconsideration is respectfully requested.

The claims are 1 to 12.

Claims 1 to 12 have been rejected as anticipated by or unpatentable over Obuchi et al. (U.S. '294).

This rejection is respectfully traversed.

As recognized in the first part of paragraph 2 of the Official Action, Obuchi et al. (U.S. '294) discloses an item formed from aliphatic polyester (col. 1, lines 10 to 12), to which a transparent nucleating agent has been added in order to improve thermal resistance through an increase in crystallinity (col. 2, lines 26 to 27).

In rejecting claims 1 to 12 in paragraph 2., it is asserted:

It is known in the art that stretching a material will increase the crystallinity of said material . . . The materials will have a higher crystal melting point than that of an un-stretched or untreated product. It is the Examiner's view that the stretched product having a higher crystal melting point by at least 5°C would be inherent given that the purpose of stretching the product is to improve the crystal melting point.

In reply, it was not believed to be known in the art that stretching will increase the crystal melting point or substantially modify the viscoelastic properties of a crystalline thermoplastic resin. Rather, it was believed in the art that an increase in crystallinity of a crystalline thermoplastic resin will not substantially influence (but rather lower) the crystal melting point or the viscoelastic properties of the resin. In support of this belief, please see the following two references (copies enclosed): Ref. 1: Z.M.O. Rzaev, et al. "A One-Step Preparation of Compatibilized Polypropylene - Nanocomposites by Reactive Extrusion Processing", Advances in Polymer Technology, Vol. 26, No. 1, pages 41-55 (2007); and Ref. 2: Ryohei Fukae et al., "Dynamic Viscoelasticity of Syndiotactic Poly(vinyl alcohol) Derived from Vinyl Pivalate" SEN'I GAKKAISHI (Journal of the Fiber Science & Technology, Japan), Vol. 53, No. 5, pages 195-203 (1997).

Ref. 1 in TABLE II at page 47 shows some correlation between crystallinity and crystal melting of Nanocomposites - 1 to 3. Nanocomposite-1 is a nanocomposite of i-PP (isotactic

polypropylene) 80 wt%, oligo[i-pp-g-MA (0.15 mol%)] (i-PP oligomer grafted with 0.15 mol% of maleic anhydride) 15 wt% and organo-MMT (dodecylamine-surface-modified montmorillonite) 5 wt% obtained through reactive extrusion. See ABSTRACT at page 41 and page 46, right col., lines 7 to 13. Similarly, Nanocomposite-2 is a nanocomposite of i-PP 80 wt%, oligo[i-pp-g-MA (0.86 mol%)] 15 wt% and organo-MMT 5 wt% , and Nanocomposite-3 is a nanocomposite of i-PP 80 wt%, oligo[i-pp-g-MA (1.22 mol%)] 15 wt% and organo-MMT 5 wt%.

TABLE II of Ref. 1 shows that a DSC-crystallinity increase from 34.6% (of Nanocomposite-3) to 41.2% (of Nanocomposite-1) is accompanied with only a decrease of Tm (crystal melting point) of from 163.3°C to 162.4°C. On the other hand, a DSC-crystallinity increase from 31.3% (of virgin i-PP) to 41.2% (of Nanocomposite-1) is accompanied with a decrease of Tm of from 167.5°C to 162.4°C.

From the above, it is clear that the increase in crystallinity does not necessarily result in an increase in crystal melting point.

Ref. 2, in Table 2 at page 196, shows that st-L(1), st-L(2) and st-L(3) (i.e. st-L (PVA(polyvinyl alcohol))) with syndiotacticity of 61% (page 196, left col., lines 7-6 from the bottom) annealed at different conditions (page 196, right col., 2-3 lines above Table 2 showed crystallinities of 20%, 29% and 52%, respectively.

On the other hand, Fig. 5 at page 199 shows that tan δ plots represented by O, Δ and □ of st-L(1), st-L(2) and st-L(3), respectively, showing dispersion peaks (see page 19, lines 4 to 19 of the present specification) around 60°C. The dispersion temperatures are not substantially different, and especially it is noted that the plots represented by Δ and □ of st-L(2) (showing crystallinity of 29%) and st-L(3) (showing crystallinity of 52%) substantially overlap each other, i.e. show identical dispersion temperatures.

The above data also shows that an increase in crystallinity is not necessarily accompanied by an increase in dispersion temperature.

Thus, the underlying assumption in rejection of claims 1 to 12 is unfounded.

In contrast, the present invention is based on the discovery that crystalline aliphatic polyester subjected to intense stretching causes a substantial increase in crystal melting point, main and sub-dispersion peak temperature according to dynamic viscoelasticity measurement, which lead to substantial improvements in retort-durability, gas-barrier property and strength. The intense stretching conditions are represented by a large stretch ratio in excess of 3 times at least in a uniaxial direction, preferably in excess of 3 times in each of biaxial directions, and a relatively low stretching temperature of below 80°C, preferably 45 to 60°C (page 15, lines 4 to 23 of the present specification) relative to a glass transition temperature of the resin (e.g. ca. 38°C for glycolic acid homopolymer as described at page 11, lines 24 to 25).

For example, the effect of the intense stretching for glycolic acid homopolymer cannot be attained at biaxial stretching ratios of 3x3 times at 45 - 80°C (Comparative Examples 1 to 3) or 4x4 or 4.5x4.5 times at 80°C (Comparative Examples 4 and 5). See Tables 1 and 2 at page 24 of the present specification.

In Section 4 of the Official Action, in rejecting claims 1 to 12, it is asserted:

However, the conditions in which the films were stretched for Obuchi et al. and the Applicant are the same, thus the physical properties would be the same for the final film. (emphasis added).

This is rejection is also untenable.

As has been recognized by the Examiner, Obuchi et al. discloses that a container was formed from an injection molding machine and was blown to expand twice in both the longitudinal and transverse directions (col. 27, line 43 et seq.). The biaxial stretching ratios of 2x2 times are substantially smaller than biaxial stretching ratio in excess of 3x3 times adopted in the present invention, and the expansion was effected at 120°C which is substantially higher than the glass transition temperature of 59°C of an identical material (in Example 3-1 at col. 23, line 39) compared with the stretching temperature of below 80°C, preferably 45 to 60°C, relative to the glass transition temperature of ca. 38°C of glycolic acid homopolymer adopted in the present invention. Thus, Obuchi et al. does not disclose intense stretching conditions comparable to those adopted in the present invention.

- 4 -

Consequently, Obuchi et al. fails to disclose or suggest a stretched aliphatic polyester product having a substantially increased crystal melting point and substantially increased main and sub-dispersion temperatures than those of an un-stretched product thereof obtainable through intense stretching of a crystalline aliphatic polyester resin.

For the foregoing reasons, the rejections on Obuchi are untenable and should be withdrawn.

No further issues remaining, allowance of this application is respectfully requested.

If the Examiner has any comments or proposals for expediting prosecution, please contact undersigned at the telephone number below.

Respectfully submitted,

Daisuke ITOH et al.

By:_____

Matthew M. Jacob
Registration No. 25,154
Attorney for Applicants

MJ/aas
Washington, D.C. 20006-1021
Telephone (202) 721-8200
Facsimile (202) 721-8250
December 17, 2007

A One-Step Preparation of Compatibilized Polypropylene-Nanocomposites by Reactive Extrusion Processing

Z. M. O. RZAEV, A. YILMAZBAYHAN, E. ALPER

Department of Chemical Engineering, Faculty of Engineering, Hacettepe University, 06800 Ankara, Turkey

ABSTRACT: We have developed a one-step method for preparing nanocomposites based on powdered isotactic polypropylene (i-PP) as a matrix polymer (melt-flow index (MFI) = 7.2 g 10 min^{-1}), oligo(i-PP-g-MA) (MFI = 35–70 g 10 min^{-1}) as a reactive compatibilizer and docecylamine-surface-modified montmorillonite clay (organo-MMT). This method includes grafting maleic anhydride (MA) onto i-PP chains in the melt state under the controlled thermal degradation conditions and intercalative compounding of the obtained oligo(i-PP-g-MA) with i-PP and organo-MMT by reactive extrusion. The effect of extrusion parameters on MFI, composition and properties of the grafted i-PPs, and mechanism of formation and properties of PP/oligo(PP-g-MA)s/organo-MMT nanocomposites were investigated by FTIR, XRD, and thermal analysis (DSC, TGA, and DTA). The results indicate that the formation of nanostructured morphologies proceeds through the formation of

WILEY
InterScience®
DISCOVER SOMETHING GREAT

Introduction

I n the last decade, the attention of many scientific and industrial researchers has focused on thermoplastic and thermoset polymer silicate layered nanocomposites (PLSs). This considerable scientific and engineering interest has been stimulated by the possibility of obtaining significant improvements in physical, mechanical, thermal, and functional properties of PLS materials. The results of these researches are summarized and discussed in several reviews[1-4] and a book.[5] The most promising composite systems are nanocomposites based on organic polymers, including maleic anhydride (MA) grafted polyolefins, and inorganic clay minerals consisting of silicate layers.[6-9] In clay structures of the montmorillonite (MMT) type, the single silicate layers have a thickness of about 1 nm and typically lateral dimensions of several hundred nanometers up to micrometers. These layers are arranged in stacks with regular interstices called *interlayer galleries*. To enable the formation of a nanocomposite structure, through the intercalation of polymer chains in these interlayer galleries, an organomodified clay material has to be used in which the counterions of the silicate layers (typically Na^+, Li^+, Ca^{2+}) situated in the interstitial regions are exchanged with bulky alkylammonium ions.[10,11] Such organo-modified clays are available commercially in several varieties, tailor made for different applications and are compatible with many polymeric materials. Therefore, process monitoring during preparation and characterization of the resulting nanocomposite materials is of increasing importance.[12] Because of the small dimensions of the filler particles and the resulting high surface-to-volume ratio, nanocomposites are effective even at low-filler concentrations. A high fraction of interfacial regions (interphase) is required to achieve broad physical properties and therefore the material performance.[13]

Usuki et al.[6-9] found that functionalized polyolefins fitted quite well into the galleries of organophilic clay, and they successfully prepared polypropylene (PP)-clay nanocomposites based on MA-modified PP and organophilic clay.[7,8,12] In PP-clay nanocomposites, the silicate layers of the organophilic clay exfoliate and homogeneously disperse at the nanometer level in the PP matrix. The methodology of grafting MA units to nonpolar polymer chains is applicable to other polyolefins, such as PE, poly(E-co-P), and poly(E-co-P-co-diene) rubbers.[9] Thus, E-P rubber-clay nanocomposites were prepared by melt-compounding poly[(E-*co*-P)-*g*-MA] with organophilic clay and their properties were examined. Silicate layers of used clay were found to exfoliate and homogeneously disperse at the nanometer level into the nanocomposites as shown by transmission electron microscopy. It is thought that MA units (or maleic acid groups generated by hydrolysis) grafted to the E-P polymer chains are selectively absorbed onto the dispersed silicate layers and form strong ionic interaction, because MA units have good affinity to ionic surfaces of silicate layers. According to several authors, the silicate layers, dispersing at the nanometer level, provide large pseudo-cross-links within the polymer and improve the creep resistance of nanocomposites. Nanocomposite technology is very useful to improve the properties of thermoplastic elastomers via the usage of small amount of silicate layers loaded with or without conventional fillers such as carbon black and talc.[9]

The preparation of poly(PP-*g*-MA)-based nanocomposites was described in detail by Böhning et al.[12] and Tidjani et al.,[14] who discussed the influence of oxygen on the melt-blending/preparation, causing a partial degradation of the organic cations used to modify the clay surface and a decrease in thermal stability of the resulting polymer/layered silicate nanocomposites. Three types of poly(PP-*g*-MA)-layered silicate nanocomposites with different

dispersion states of layered silicate (de-intercalated, intercalated, and exfoliated states) have been prepared from two kinds of PPs, having different molecular weights.

The effect of the final morphology of the nanocomposites has been studied on the basis of rheological and mechanical properties[15] and dielectric relaxation[12] for the organically modified silicate layers. The results of nonisothermal crystallization kinetics of PP and poly(PP-g-MA) nanocomposites studied by differential scanning calorimetry (DSC) at various cooling rates have indicated that maleated PP can accelerate the overall nonisothermal crystallization process of PP.[16]

MA—styrene/silica hybrid material has been successfully prepared from random poly(MA-rand-methyl methacrylate), ternary poly(MA-co-trans-stilbene-co-n-butyl methacrylate),[17] and alternating poly(MA-alt-styrene)[18] copolymers and tetraethoxysilane (TEOS) in the presence of 3-aminopropyltriethoxysilane (APTS) as a coupling agent by in situ sol-gel process. These systems can be described as appropriate models for polymer/organo-MMT nanocomposite system in which APTS plays the role of organo-silicate. The covalent bonds between organic and inorganic phases were introduced by the aminolysis reaction of amine group with MA units of copolymer to form a copolymer bearing $(C_2H_5O)_3Si$ groups, which undergoes hydrolytic polycondensation with TEOS and forms silicate-type structure.[17,18]

The attractive characteristics of polymer–clay nanocomposites include high-mechanical properties and thermal resistance,[19–22] low flammability,[23–25] gas barrier properties,[26–29] and corrosion protection effects.[30,31]

The preparation of new functional monomers is also an effective way to develop polymeric materials with dramatically improved properties. In last years, the formation of polymer-based organic-inorganic nanocomposites has attracted extensive interest as it is an economic and simple way to enhance polymer properties.[5,32] Parija et al.[32] have studied the physico-mechanical and thermal properties of PP/layered silicate nanocomposite prepared from blends of PP-95 (MFI g 10 min^{-1}), poly[PP-g-MA(1%)]-2 as a compatibilizer and octadodecylamine-modified MMT-3 as a reinforcing agent. This nanocomposite showed improved thermal and mechanical (specific gravity) properties and delayed crystallization as compared to virgin PP.

Recently, we have reported the synthesis of poly(PP-g-MA)s with different compositions as the precursor for the preparation of nanocompos-ites by radical grafting reaction of powder and granular PP with MA by reactive extrusion.[33–36] It was demonstrated that the structure, crystallinity, crystallization, and thermal behavior of PP changed with grafting and depended on the grafting degree. The results of grafting of MA onto powder PP in the thermal oxidative conditions of powder PP were also reported.[36] The present work concerns with the synthesis and characterization of (i-PP)/oligo(i-PP-g-MA)s/organo-MMT silicate nanocomposite including (1) preparation of oligo(i-PP-g-MA)s with different compositions, by grafting MA onto i-PP powder using twin-screw reactive extrusion under controlled degradation conditions and their characterization; (2) one-step production of nanocomposites in the melt state by reactive extrusion, including controlled degradation–grafting–compounding, under specific processing conditions; (3) study of nanocomposite composition–property relationship (thermal and crystallization behavior and X-ray diffraction parameters); and (4) analysis of various models and mechanism for the formation of the intercalated and exfoliated nanostructures through H-bonding and amidization/imidization in situ reactions.

Experimental

MATERIALS

The isotactic polypropylene (i-PP) powder was supplied by Petkim Petrochemical Holding Inc. (Izmir, Turkey) taken directly from the polymerization reactor. It has properties similar to the commercial granular i-PP, having M_w 53,300 g mol^{-1}, M_n 24,300 g mol^{-1}, polydispersity index (PI) = 2.19, melt-flow index around 7.2 g 10 min^{-1} (230°C and 2.16 kg), melting point (T_m) 167.5°C, and crystallinity 31.3% (by DSC). The maleic anhydride monomer (MA) (Fluka, Switzerland) was purified before use by recrystallization from benzene solution and by sublimation under vacuum. This has a melting point equal to 52.8°C. The initiator dicumyl peroxide (DCP) (Perkadox BC-FF, Akzo Nobel Chemicals Inc., Holland) and solvents (toluene, methanol, and 1,2,4-trichlorobenzene (TCB)) were used without further purification. Other additives such neutralizer (calcium stearate) (I), antioxidants and stabilizer [tetrakis methane (II), tris(2,4-di-tert-butylphenyl) phosphate (III), and tris(3,5-di-tert-butyl-4-hydoxybenzyl)isocyanurate (IV)] were

supplied by Petkim Petrochemical Co., which are mixed with the i-PP powder before the reactive extrusion of nanocomposite components. The MA-grafted i-PP has a very high MFI value (approximately five times greater than the value of the original i-PP) and a very low molecular weight ($M_n \leq 10,000$ g mol^{-1}) (for this reason, it has been referred as "oligomer"). The compatibilizer oligo(i-PP-g-MA) was prepared by grafting MA onto i-PP chains under thermal degradation conditions using the reactive extrusion. Various oligo[i-PP-co-MA(0.15–1.22 mol%)] systems produced had the following characteristics: carboxylic acid content (expressed as acid number, defined in Eq. (1)) within the range 8.0–32, MFI in the region 35.2–61.0 g 10 min^{-1}, and $T_m = \sim 161$°C. Dodecylamine surface modified organo-MMT silicate (Viscobent SB-1) was supplied by Bensan Activated Bentonite Co. (Istanbul, Turkey) and/or prepared by using the well-known method.[10]

REACTIVE EXTRUSION PROCESSING

A purpose-designed laboratory-sized twin-screw extruder was used for all the preparations, including oligo(i-PP-g-MA) and its blends with i-PP and organo-MMT. The ratio of length to diameter (L/D) was 13.35. The extrusion temperature was set at 165–180°C. Screw speed was fixed at 14–30 rpm, and grafting and compounding processes were carried out under both air and nitrogen atmospheres. Prior to blending, the powdered i-PP and organo-MMT samples were dried at 60°C for 6 h. Before the preparation of i-PP nanocomposites, dried powdered i-PP was mixed with various stabilizers and additives (I–IV) as recommended by the producer (Petkim Petrochemical Holding Inc.) in the following amounts related to 1 g of i-PP: 500 (I), 470 (II), 312 (III), and 312 ppm (IV). The premixed powder was consequently mixed with specified amounts of MA-grafted compatibilizer and organo-MMT.

REACTIVE GRAFTING COMPOUNDING

Both the grafting and in situ modification reactions were carried out in the melt by using a purpose-designed laboratory-sized twin-screw extruder. The temperature profile of the extruder zones was 165, 170, 175, and 180°C; grafting of MA onto the i-PP polymer was carried out in a wide range of i-PP/MA/DCP ratios in air under controlled degradation conditions using virgin i-PP powder, while the preparation of the i-PP80/oligo(i-

PP-g-MA)s15/organo-MMT5 nanocomposite was realized under nitrogen atmosphere, using compounded i-PP and MA-grafted i-PPs with different grafted unit contents (0.15, 0.86, and 1.22 mol%). The MA-grafted oligomer was dissolved in TCB at 150°C and precipitated with methanol at 80–100°C, and than dried under vacuum at 100°C for 24 h. The grafted i-PP was also prepared and characterized separately in order to study the first process, due to difficulty of separating it from the overall compounded system.

MATERIAL CHARACTERIZATION

Fourier transform infrared (FTIR) spectra of the nanocomposites (KBr pellet) were recorded with an FTIR Nicolet 510 spectrometer in the 4000–400 cm^{-1} range, taking 30 scans at 4 cm^{-1} resolution.

The carboxylic acid number of grafted copolymers was determined by a standard titration method, using Eq. (1), and converted into the MA content. The grafting efficiency is expressed as wt% grafted MA units on i-PP, calculated from the obtained acid number value, i.e.

Carboxylic acid number (mg KOH/g polymer)

$$= 56.1(N_1 V_1 - N_2 V_2)/m \qquad (1)$$

where N_1 and V_1 are the normality (0.0909 N) and amount (mol L^{-1}) of the added titrant KOH solution in methanol, and N_2 and V_2 are the normality (0.096 N) and amount (mol L^{-1}) of HCl solution, used to neutralize the excess KOH, and m (g) is the weight of the polymer sample.

The thermal characteristics of the grafted copolymers, including melting point temperature (T_m), crystallization temperature (T_c), degree of crystallinity (χ_c), and thermal stability (T_d) were determined by DSC and differential-gravimetric thermal (TGA-DTG) analysis methods. The thermal behavior of the copolymers was assessed with a Shimadzu calorimeter (Japan) and Setaram Labsys TG-DTA 12 thermal analyzer (France), under nitrogen atmosphere at a heating and cooling rate of 10°C/min. The area under the melting peak was taken to be the melting enthalpy. The crystallinity of the graft copolymers and nanocomposites was determined using Eq. (2):[37]

$$\text{Crystallinity (\%)} = (\Delta H_f / \Delta H_f^o) \times 100 \qquad (2)$$

where ΔH_f is the melting enthalpy of copolymers or nanocomposite, and ΔH_f^o is the enthalpy of 100% crystalline PP ($\Delta H_f^o = 209$ J g^{-1}).[38]

The ratio of crystalline/amorphous phase contents in the graft oligomers and nanocomposites was determined by X-ray powder diffraction (XRD) analysis using Rigaku D-MAX 2200 diffractometer (Japan) employing Cu Kα ($\lambda = 1.54059$ Å) radiation over the range $5° \leq 2\theta \leq 50°$. The crystallinity of the graft copolymers and the corresponding nanocomposites was calculated using the following equation:[39]

$$\chi_c = \int_0^\infty s^2 I_c(s)d \bigg/ \int_0^\infty s^2 I(s)d \qquad (3)$$

where s is the magnitude of the reciprocal-lattice vector which is given by $s = (2 \sin \theta)/\lambda$, θ is one-half the angle of derivation of the diffracted rays from the incident X-rays, and λ is the wavelength; $I(s)$ and I_c (s) are intensities of coherent X-ray scattering from both crystalline and amorphous regions and from only crystalline region of polymer sample, respectively, and d is the interlayer spacing.

MFI values (g 10 min^{-1}, 190°C, and 2.16 kg) were obtained using an extrusion plastomer (ATS FAAR, Vignate, Italy).

Results and Discussion

GAFTING-OLIGOMERIZATION AND PREPARATION OF NANOCOMPOSITES

The grafting of MA onto i-PP polymer chains was carried out in the melt by reactive twin-screw extrusion in the presence of DCP as an initiator. The effect of [DCP] initiator and [MA] monomer concentrations, i.e., i-PP/MA/DCP feed ratio, on the grafting degree is shown in Figs. 1 and 2.

The plots of grafted MA versus [DCP] (Fig. 1) indicate that the extent of grafting is significantly reduced at high DCP concentrations (>3 wt%), probably due to the occurrence of side reactions, such as chain scission. The most efficient grafting reaction occurred at [DCP] around 2–3 wt% and [MA] around 2–4 wt%, respectively. As seen from Fig. 2 with the MA concentration in the range 1.0–4.0 wt%, effective grafting only takes place at relatively lower DCP concentrations, 0.5–1.0 wt%. These results in-
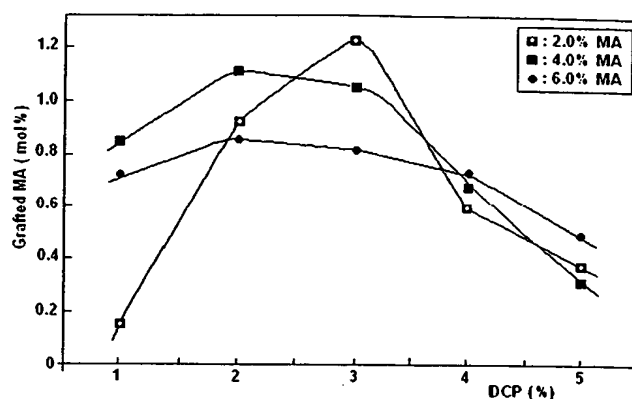

FIGURE 1. Effect of DCP initiator concentration on the grafted degree at constant MA concentration.

dicated that MA/DCP weight ratio around 0.4–1.0 in i-PP/MA/DCP mixtures gives the highest level of grafting under the chosen extrusion conditions.

The MA/DCP weight ratio also affects the MFI values of the resulting grafted polymers. As shown in the [MFI] versus [MA] plots (Fig. 3), chain scission reactions are significantly suppressed at 3.0 wt% MA concentrations, especially when more than 1.0 wt% of DCP initiator is used. For MA concentrations greater than 3 wt%, a decrease in MFI is dominant event. High rate of degradations (increase in MFI value) is only observed when 0.5 wt% of DCP and 1.0 wt% of MA are used in the i-PP/MA/DCP mixture. We also studied the degradation of powdered
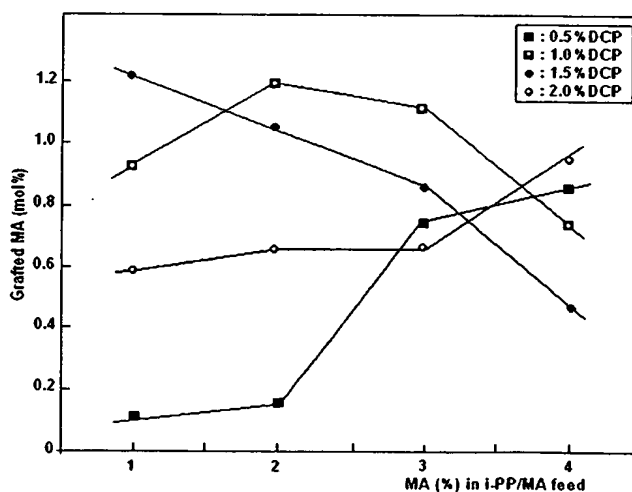

FIGURE 2. Effect of MA concentration on the grafted degree at constant DCP concentration.
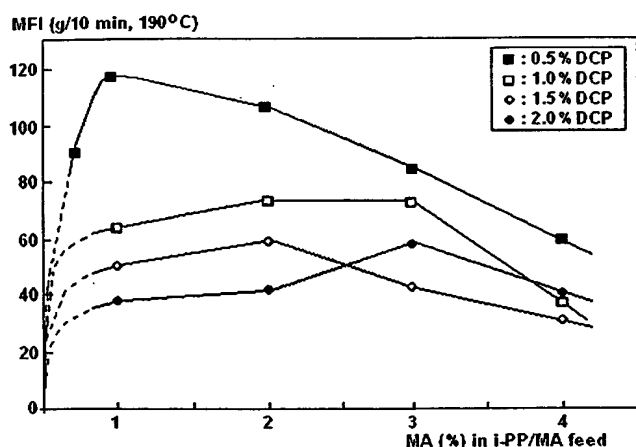
MFI (g/10 min, 190°C)

FIGURE 3. Effect of MA and DCP concentrations on the MFI parameters of oligo(i-PP-g-MA)s.

i-PP (MFI $= 7.2$ g 10 min^{-1}), which does not contain any processing stabilizer. In order to elucidate the effect of DCP concentration on the MFI of i-PP in the absence of MA-grafted agent, under similar extrusion conditions, the obtained results are summarized in Table I. As seen from these data, thermal oxidative degradation can occur even in the absence of DCP, resulting in an increase in the MFI up to the value of 78. It was observed that an increase in DCP amount from 0.5 to 4.0 wt% significantly decreased the degradation parameter (A), as defined in the footnote of Table I, and MFI value of degraded i-PP increased fourfold. This is not a controllable process and essentially depends on many factors,

TABLE I ▬

Effect of DCP Content on the Thermal Degradation of i-PP (as a function of MFI) in the Absence of MA-Grafting Agent in Given Extrusion Conditions

DCP (wt%)	Barell Temperature (°C)	Screw Speed (rpm)	(MFI)$_1$ (g 10 min^{-1})	A^*
0.0	175	30	78	1.0
0.5	175	30	180	0.43
1.0	175	30	218	0.36
1.0	180	14	234	—
1.0	190	14	243	—
1.5	175	30	270	0.29
2.0	175	30	300	0.26
2.0	175	14	210	—
4.0	175	30	310	0.25

*$A = $ (MFI)$_0$/(MFI)$_1$ is degradation parameter. (MFI)$_0$ is the MFI value of thermally degraded PP without DCP.

such as temperature, screw speed, and other extrusion parameters. The introduction of MA into this system allows the process to reasonably control the chain degradation reactions (Fig. 3).

THERMAL CHARACTERISTICS AND CRYSTALLINITY

The formation of intercalated/exfoliated nanocomposite structures was confirmed by the comparative FTIR, XRD, and DSC analyses of the system i-PP-80 (wt%)/oligo[i-PP-g-MA(X mol%)]-15 wt%/organo-MMT-5 wt% (where X $= 0.15$, 0.86, and 1.22 mol% for nanocomposites 1, 2, and 3, respectively) and their respective components.

The results of MFI, DSC, and XRD measurements for the nanocomposites and their individual components are presented in Tables II and III. As can be seen from the comparative analysis, the MFI values of both the nanocomposites and the graft oligomers largely depend on the content of MA units. The MFI decreases on increasing the MA-grafting fragment or MA monomer concentration in the i-PP/MA mixture (Fig. 3). The DSC curves for oligo(i-PP-g-MA) systems (Fig. 4) and their nanocomposites
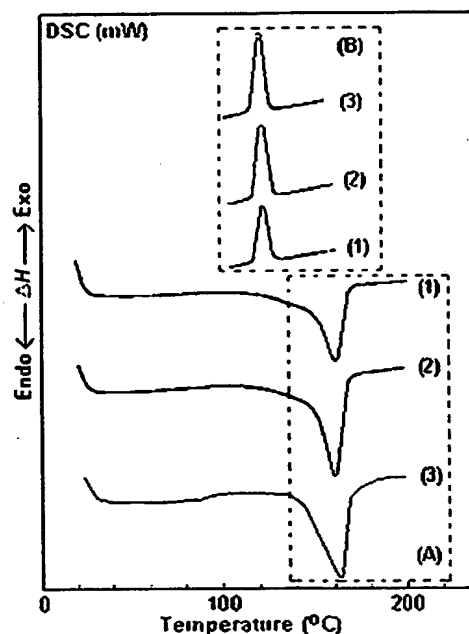

FIGURE 4. DSC scans of oligo[i-PP-g-MA(X mol%)]s at heating/cooling rate of 10°C/min under nitrogen atmosphere: (A) melting and (B) recrystallization regions for grafted PP with X $= 0.15$ (1), 0.86 (2), and 1.22 (3) mol%.

TABLE II ■

Some Characteristics of PP(80)/Oligo(PP-g-MA)(15)/MMT(5) Nanocomposites and Their Individual Components

Nanocomposites and Their Individual Components	—COOH (wt%)	MFI (g 10 min⁻¹, 190°C)	T_m(°C)	ΔH (J g⁻¹)	T_c(°C)	ΔH (J g⁻¹)	Crystallinity χ_c(%) DSC	XRD
Nanocomposite-1	–	24.5	162.4	86.0	114.3	83.3	41.2	44.7
Nanocomposite-2	–	21.0	162.1	73.1	115.1	82.1	35.0	43.3
Nanocomposite-3	–	18.8	163.3	72.3	115.5	81.2	34.6	42.1
Isotactic PP (powder)	–	7.2	167.5	67.7	102.6	64.5	31.3	30.6
Oligo[i-PP-g-MA(0.15 mol%)]	8.00	61.0	161.0	86.4	119.5	67.1	41.3	40.7
Oligo[i-PP-g-MA(0.86 mol%)]	22.65	38.2	160.5	74.7	119.7	63.5	35.7	35.8
Oligo[i-PP-g-MA(1.22 mol%)]	32.15	35.2	161.5	68.6	120.9	68.7	32.8	33.0

(Fig. 5), related to melting and recrystallization events, showed that the T_m and T_c values and enthalpy (ΔH) of these transitions depend on the grafting degree of the copolymers (Table III). These parameters, however, did not change significantly by increasing the MA content of the copolymer in the nanocomposites. In any case, the observed difference between the crystallization temperature values ($\Delta = T_m - T_c$) for virgin i-PP (54.9 °C) and nanocomposites (47.6°C average value) is significant, indicating that the recrystallization process proceeded

relatively rapidly in the case of nanocomposites, as compared to virgin i-PP and its grafted copolymers. This can be explained by the ease of reorientation of nanostructural fragments in the i-PP-80/oligo(i-PP-g-MA)-15/organo-MMT-5 nanocomposites. Furthermore, the crystallinity (χ_c) of nanocomposites, calculated from DSC (enthalpy values of melting, ΔH) and XRD patterns (Table III), is higher (around 42–45%) than those for i-PP (30.6%) and its grafted oligomers (around 33–41%) (Table II). This is a reasonable argument for the hypothesis regarding the

TABLE III ■

XRD Parameters of Compatibilized i-PP-Nanocomposites with Given Composition as in Table II

Nanocomposite Components	MA Unit (mol%)	Intensity of Peak (Counts)	2θ (Degree)	d (Å) (Interlayer Spacing)	Crystallinity χ_c (%)
Nanocomposite-1					44.7
Propylene units[a]		4260	14.2	6.19	22.6
		2663	22.0	4.04	
MA-grafted units	0.15	2441	16.5	5.21	3.3
Organo-MMT		1376	9.9	4.72	18.8
silicate layer		4704	2.3	31.99	
Nanocomposite-2					43.3
Propylene units		3167	14.2	6.20	20.0
		2566	21.9	4.06	
MA-grafted units	0.86	1833	16.5	5.23	5.6
Organo-MMT		1133	9.8	4.76	17.7
silicate layer		3833	2.3	34.76	
Nanocomposite-3					42.1
Propylene units		2869	14.2	6.17	19.1
		2386	21.9	4.07	
MA-grafted units	1.22	1590	16.5	5.19	6.4
Organo-MMT		937	9.9	4.74	16.5
silicate layer		3665	2.3	33.57	
Organo-MMT		207	9.9	9.97	58.2
silicate layer (virgin)		2759	3.5	25.10	

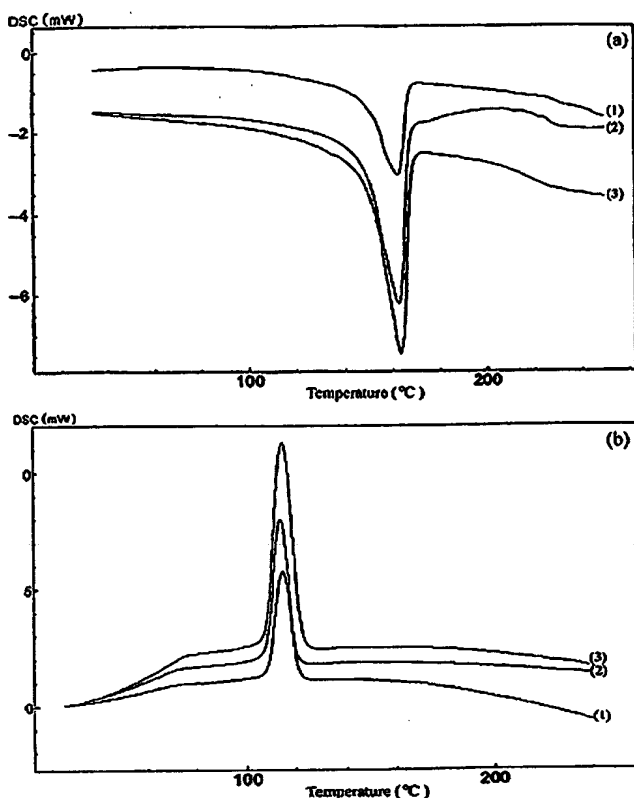[a]Propylene units from PP matrix and/or from grafted PP.

FIGURE 5. DSC scans of (a) melting and (b) recrystallization process of the nanocomposites at heating/cooling rate of 10°C/min under nitrogen atmosphere: Content of oligo[i-PP-g- MA(X mol%)]s is constant (15 wt%). X values are given in Fig. 4.

formation of a highly oriented nanostructural architecture in the nanocomposites. As evidenced from the data in Table II, some discrepancy occurs between the crystallinity values (χ_c) obtained from DSC and XRD data for the studied nanocomposites. The difference, $\Delta = \chi_c$ (XRD) $- \chi_c$ (DCS), is 3.5% for nanocomposite-1 containing reactive compatibilizer with a lower amount of MA-grafted units (0.15 mol%) and ~8.0% for nanocomposites-2 and -3 containing compatibilizer with a relatively higher amount of MA-grafted units (0.86 and 1.22 mol%, respectively). This observed phenomenon can be explained by the probable specific mechanism of recrystallization processes at nanodimension levels in the melting–cooling runs of the DSC analysis (under nitrogen atmosphere). This is the case especially for the nanocomposites containing the higher amounts of grafted MA units. The χ_c values for powdered samples were obtained at room temperature. It can be assumed that a relatively lower amount of grafted

unit and its rearranged strong polar derivatives can play the role of nucleating centers in the recrystallization process, as confirmed by the highest χ_c values obtained from both DSC and XRD analyses, as well as, the visibly evident, less degraded nanocomposites containing lower amounts of anhydride units in compatibilizer (Fig. 6).

The results of the TGA–DTA analysis (Fig. 6) show that the nanocomposites undergo a one-step degradation process and exhibit higher thermal stability up to 420°C, as compared with virgin i-PP (Fig. 6, curve 4). The observed endothermic peaks around 162–165°C in the DTA curves, associated with melt transition state of crystalline structures, are similar to those determined by the DSC method (Fig. 5).

NANOSTRUCTURE

The results of the FTIR spectral analysis of nanocomposites and their individual components including the characteristic absorption bands and their assignments are summarized in Table IV. The appearance of the characteristic bands at 1845–1710 cm^{-1} is associated with C=O symmetric and antisymmetric C=O bands in the grafted anhydride unit. A quantitative chemical analysis of these groups was carried out by titration. The values of the acid number (i.e., the carboxylic acid content) derived from the grafted MA units are presented in Table II. The formation of intercalated nanostructural linkages (H-bonded macrocomplexes and amide/imide groups) can be confirmed by the presence of the following characteristic absorption bands (Fig. 7, Table IV): (1) 2450 (w) and 960 cm^{-1} (w) for OH stretching and deformation bands, respectively, in —COOH groups occurring after amidization, (2) 3460 (very broad, s) and 3250 cm^{-1} (w) for H-bonded NH$_2$ or OH stretching in complexed graft linkages, (3) 2500–2300 (w) and 1550 cm^{-1} (w) for C—NH$_3^+$.$^-$OOC— complex or —COO$^-$ stretching and 500 (m.—s), 560 cm^{-1} (m) for —COO$^-$ rocking, and (4) 1640 (m) and 1590 cm^{-1} (w) for C=O amide or imide stretching.

The XRD analysis was employed to check the effect of grafting on the crystallization and formation of nanostructural linkages. The results of the comparative XRD analysis of nanocomposites and their individual components are illustrated in Figs. 8 and 9 and are summarized in Table III. The following changes in XRD patterns were observed: (a) increase in the d-spacing of a strong silicate peak as compared to the original organo-MMT clay from 25.08 to 34.76 Å values, (b) shift of this peak to lower
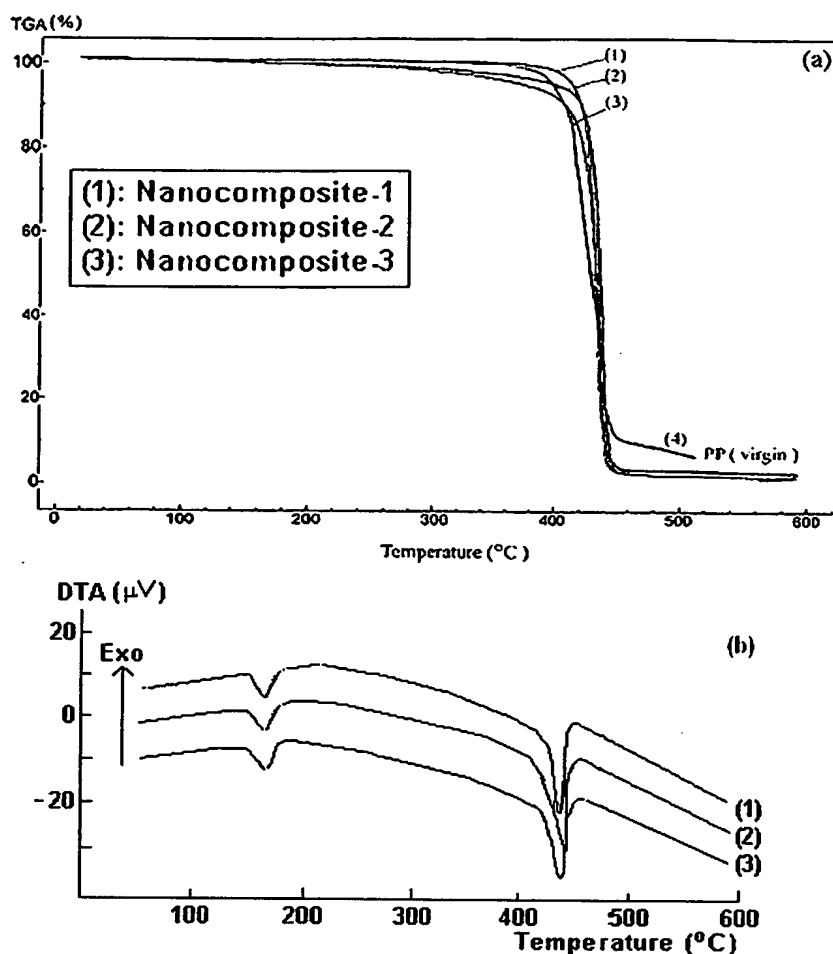
FIGURE 6. TGA (a) and DTA (b) curves of *i*-PP80/oligo[*i*-PP-*g*-MA(X mol%)]s15/organo-MMT5 nanocomposites with different grafted MA units content. Heating rate of 10°C/min under nitrogen atmosphere. X values are given in Fig. 4.

position of 2θ (from 3.47° to 1.56°), (c) characteristic XRD peaks for the *i*-PP chain in nanocomposite appear in the relatively narrow forms with high intensity, and (d) visible changes in XRD parameters by increasing MA unit contents in oligo(*i*-PP-*g*-MA)s (from 0.15 to 1.22 mol%) as the reactive compatibilizers. Moreover, relatively lower molecular weight (MFI = 61.0–35.2 g 10 min⁻¹) of the grafted copolymers compared to *i*-PP homopolymer allows them to easily intercalate in silicate interlayered galleries, where their anhydride-containing macromolecules interacted with surface alkyl amine through strong H-bonding and amidization/imidization reactions in the melt twin extrusion conditions. It can be assumed that this process provides further and easier exfoliation of *i*-PP macromolecules. These physical interaction (H-bonding) and chemi-

cal (amidization/imidization) reactions can be schematically represented in the form of a structural model as shown in Scheme 1.

For instance, Usuki et al.[7,40,41] have shown that the use of MA-modified oligopropylene (M_w = 30,000 g mol⁻¹), as a compatibilizer for PP–stearyl ammonium-MMT composites, has significantly improved the dispersibility of clays in PP nanocomposites. This has resulted in an overall increase in the dynamic storage modulus.

Wouters et al.[42–44] have studied nanocomposites based on ionomeric thermoplastic elastomers compatibilized with maleated ethylene/propylene copolymers, poly[(E-*co*-P)-*g*-MA]s. These exhibited good mechanical properties, but the melt viscosities were very high due to the very strong ionic interactions. Since the poly[(E-*co*-P)-*g*-MA] component

TABLE IV ▬

Characteristic FTIR Absorption Bands and Their Assignments for *i*-PP-80/Oligo[*i*-PP-*g*-MA(1.22 mol%)]-15/organo-MMT-5 Nanocomposite

Absorption Band (cm^{-1})	Band Assignment
Propylene units	
2970–2850 (s)	CH stretching in CH_3
2940–2845 (s)	CH_2 antisymmtrical and symmetrical stretching
1470 (s), 1450 (s)	(overlooping with CH of alkyl group in
1375 (m)	alkylamine)
998 (m.–s), 974 (m.–s)	CH_2 deformation
930–795 (m)	CH_3 deformation in C—CH_3
725 (w)	CH_2 deformation (A_{998}/A_{974} is tacticity of PP)
	CH_3 rocking coupled with skeletal modes
	CH_2 rocking
Grafted MA units	
2450 (w)	OH stretching in —COOH
1940 (w)	C=O overton
1840 (w.–m)	C=O antisymmetric stretching
1770 (m), 1710 (m)	C=O symmetric stretching
1220 (w.–m), 1050 (m)	C—O—C anhydride stretching
960 (w)	C—O—H deformation
Organo-MMT fragments	
3460 (s)	NH_2 (very broad H-bonded) or OH
3250 (w)	stretching
2500–2300 (w), 1550 (w)	H-bonded NH_2 and OH stretching
	NH stretching and NH_3 deformation in
1640 (m), 1590 (w)	C—NH_3^+. ^-OOC-complex or $-COO^-$
	stretching
1095–1015 (m)	C=O amide or imide stretching and NH_2
500 (m.–w) and 560 (m)	deformation
440 (m.–s)	Si—O—Si (silicate band)
	$-COO^-$ rocking
	chain deformation of CH_2 in alkylamine (overlooping with propylene unit)

is unable to form hydrogen bonds by itself, as the grafted MA groups do not possess a H-bond donor, an equimolar amount of a primary alkyl amine was used to open the anhydride rings, thereby forming an amide–acid structure,[45,46] to provide sites for intermolecular H-bonding to cross-link the rubber. Primary aliphatic amines were used because of their fast reaction in solution with anhydride groups at low temperatures, without the need of a catalyst. The reaction with amines has been used extensively for MA copolymers, such as poly(styrene-*co*-MA),[47,48] poly(ethylene-*co*-MA),[48,49] and poly(propylene-*co*-MA),[47] usually to obtain maleimide copolymers. It is well known that the reaction of anhydride unit of MA copolymers with alkylamine proceeds via formation of an amide–acid linkage which then undergoes ring closure to form an imide structure.[50] Sun et al.[51] have thermoreversibly cross-linked a maleated ethylene/propylene copolymer [EPM-*g*-

MA (2.1 wt%)] via the reaction of grafted anhydride units with primary alkyl amines (C_{3-18}) of different lengths. They studied the mechanical properties and the effect of the type and amount of primary amine on the structure and morphology by FTIR spectroscopy and small-angle X-ray scattering (SAXS) in order to obtain an insight into the cross-linking mechanism. It was shown that the presence of microphase-separated aggregates for both the starting graft copolymer and its alkylamide–acid and salts (complexes) act as thermoreversible physical cross-links. An irreversible formation of imide groups, on the other hand, occurred for all amide-acids and amide-complexes at high temperatures, resulting in disappearance of the aggregates and a concomitant deterioration in mechanical properties.[52]

A typical XRD pattern (Fig. 9, spectra 3) of virgin organo-MMT gives two peaks at 2θ values of 3.5° and 19.7°. The diffraction maximum around
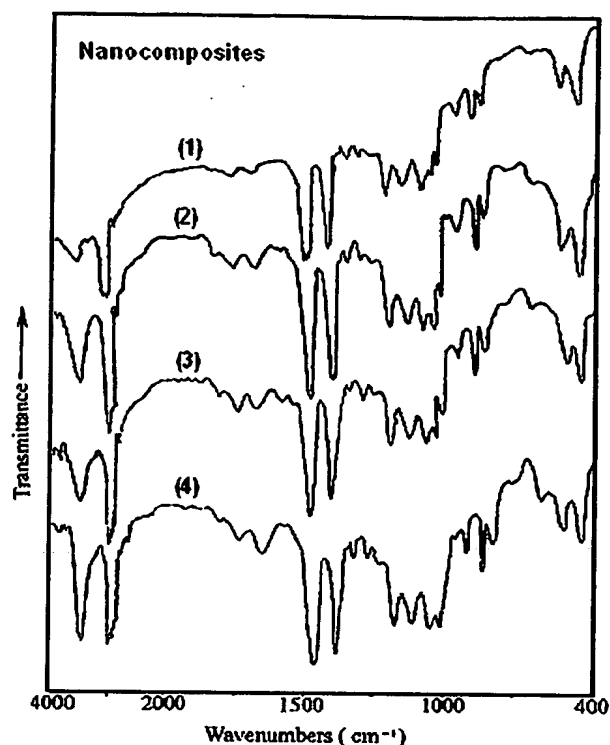
FIGURE 7. FTIR spectra of nanocomposites containing 15-wt% of compatibilizer oligo[*i*-PP-*g*-MA (X mol%)]: X = (1) 0.15, (2) 0.46, (3) 0.86, and (4) 1.22 mol%.

$2\theta = 3.5°$ is due to the (001) crystallographic plane that depends on the organo-modification of the silicate lamellae. The diffraction peak around 19.7° can be interpreted as the additional crystallographic planes inside the tetragonal and hexagonal silicate structural units. In the patterns of nanocomposites, the characteristic peak of the tetragonal unit is shifted from 3.5° (for virgin organo-MMT-docecylamine surface-modified silicate) to 2.3° (for nanocomposites), but the change in the peak position at $2\theta = 19.7°$ does not occur for the hexagonal units in the nanocomposite patterns. This confirms that the intercalation has predominantly occurred between two modified surfaces of tetragonal structural units, and significantly changed chemical structure of modified surface of silicate layers due to the interaction between anhydride units and alkylamine surface fragments. Taking into consideration the fact that the organo-MMT silicates are swelled by compounds with branched alkyl chain,[10] it can be
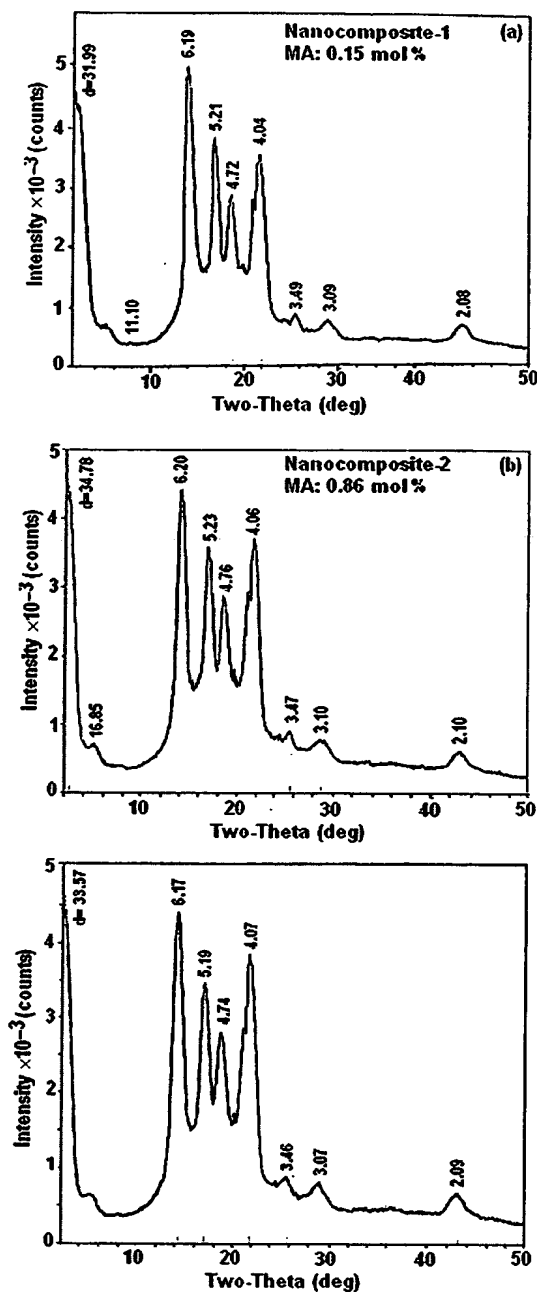

FIGURE 8. X-ray Diffraction patterns of nanocomposites: (a) *i*-PP-80/oligo[*i*-PP-*g*-MA (0.15 mol%)]-15/organo-MMT-5 (nanocomposite-1); (b) *i*-PP-80/oligo[*i*-PP-*g*-MA (0.86 mol-%)]-15/Organo-MMT-5 (nanocomposire-2); and (c) *i*-PP-80/oligo[*i*-PP-*g*-MA (1.22 mol%)]-15/organo-MMT-5 (nanocomposire-3).
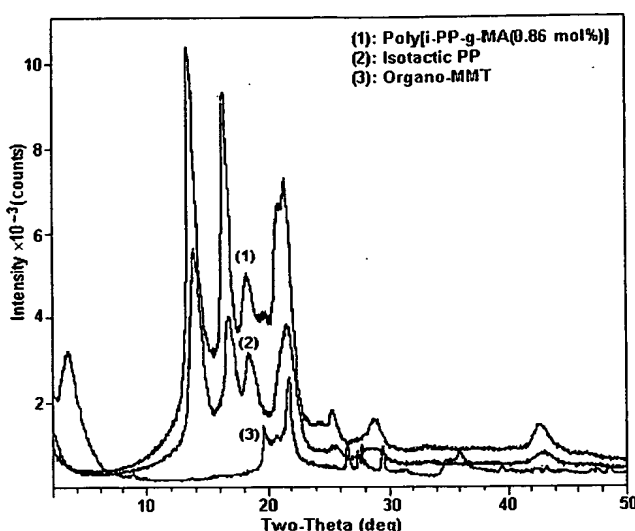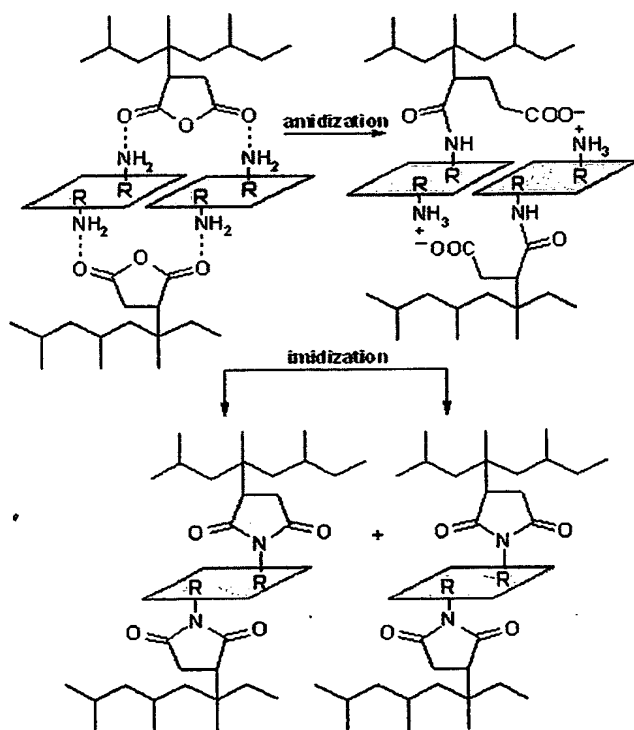
FIGURE 9. X-ray diffraction patterns of (1) poly[*i*-PP-*g*-MA(0.86 mol-%)], (2) *i*-PP, and (3) organo-MMT.


SCHEME 1 Schematic representation of in situ reactions in the formation of nanostructural architectures.

assumed that exfoliation of anhydride-containing *i*-PP chains between silicate galleries is highly probable and confirms that the orientation and interaction with alkylamine can be easily realized by melt-swelling under the chosen reactive extrusion conditions. A similar amidization/imidization reaction of anhydride-grafted units was observed in the modification of a maleated poly(E-*alt*-P) copolymer (contents of grafted MA unit 2.1 wt% and $M_n = 40,000$ g mol^{-1}) with alkyl (C$_{3-18}$) amines.[51] This can serve as a model reaction for the nanocomposites of the present study.

Lee et al.[52] examined the thermal behavior of organically modified MMT (alkylammonium cation) and its effect on the formation of PP/oligo(PP-*g*-MA(2 wt%)/organo-MMT (8 wt%) nanocomposite. They showed a decrease in interlayer spacing at processing temperatures around 180–200°C, due to release of surface organic ions by thermal decomposition. Xie et al.[53] have demonstrated that the catalytic sites on the aluminosilicate layer of organo-MMT reduce the thermal stability of a fraction of the alkylammonium ions by an average of 15–25°C. Taking into consideration the possibility of thermal degradation of the organo-MMT at the higher processing temperatures, the preparation of nanocomposites was carried out at relatively low temperatures, i.e., around 160–175°C. Contrary to the belief that the exposed surface of clay platelet may accelerate the thermal degradation of the matrix polymer,[54] due to known catalytic characteristics of the clay,[55] in this study, no thermal degradation, imposed by the modified clay surface layers, was observed for both *i*-PP and poly(*i*-PP-*g*-MA) on the basis of the MFI and TGA data.

The mechanism for the formation of the nanostructured morphologies in the preparation of nanocomposites may also be interpreted on the basis of the models by Usuki et al.[9] and Weiss,[10] according to Schemes 2 and 3, respectively.

As can be seen from Scheme 2, the polymer/organosilicate reactions can readily occur between the two alkylamine-modified surfaces and the MA-grafted copolymer in tetragonal structural units of silicate galleries. Strong H-bonding and amide/imide intermolecular linkages provide favorable conditions for the effective penetration and exfoliation processes in the formation of nanostructured morphologies. The modified Weiss model (Scheme 3) highlights the important role of the alkylamine conformation and the geometry of the modified surface in the *in situ* exfoliation and
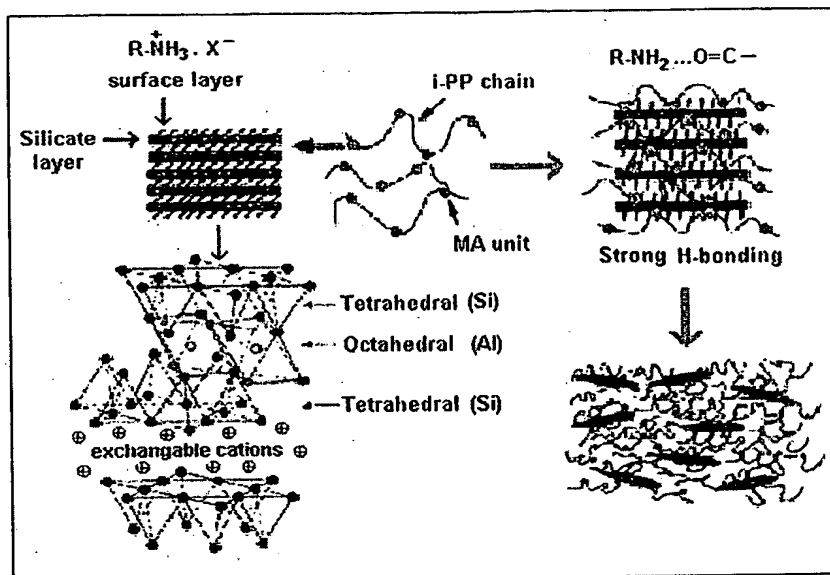
SCHEME 2 Intercalation and exfoliation of oligo(*i*-PP-*g*-MA) macromolecules in organosilicate interlayer galleries (after Usuki et al.'s model[9]). [Color figure can be viewed in the online issue, which is available at www.interscience.wiley.com.]
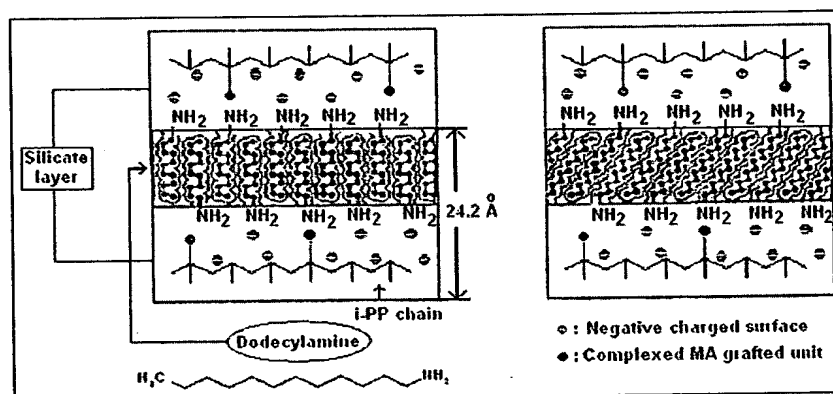
SCHEME 3 Representation of the nanostructure of *i*-PP-80/poly(*i*-PP-*g*-MA)-15/organo-MMT-5 nanocomposite using a modified Weiss model.[10] [Color figure can be viewed in the online issue, which is available at www.interscience.wiley.com.]

formation of nanostructured composites. Both of the above-described models have been used to derive a strategy for our further investigations in the field of polymer nanocomposite technology.

Concluding Remarks

This work is concerned with preparation and characterization of oligo(*i*-PP-*g*-MA)s and *i*-

PP-80/oligo(*i*-PP-*g*-MA)s-15/organo-MMT-5 nanocomposites by a twin-screw reactive extrusion under controlled degradation conditions. The effects of MA monomer and DCP initiator feed concentrations on the grafting degree, thermal behavior, and MFI in the degradation–oligomerization–grafting reactions were studied, and the optimum conditions for effective grafting of MA onto *i*-PP were determined. It was shown that grafting occurred concomitantly to controlled degradation of *i*-PP, and that a significant stabilization effect was provided by MA in the chains. The occurrence of thermal degradation

reactions was confirmed by a comparative analysis of the thermal behavior and the MFI values of both pure i-PP and its grafted derivatives. The results have shown that an increase in grafted MA content from 0.15 to 1.22 mol% decreased the T_m value of the grafted oligomer and increased the crystallization temperature. This can be interpreted in terms of a possibility of providing nucleating centers in the crystallization process of i-PP at relatively low contents of MA units. The mechanism of formation of nanostructures was explained using the results of FTIR, DSC, and XRD analyses, as well as known structural models (intercalation and exfoliation). Relatively lower molecular weight (MFI $= 61.0$–35.2 g 10^{-1} min, $M_n = 3010$–3560 g mol^{-1}) of grafted copolymers, and therefore, their relatively high-swelling capacity allows them to intercalate and exfoliate easily in silicate interlayered galleries, where the anhydride-containing macromolecules interact with the surface alkyl amine groups through H-bonding and chemical interactions (amidization/imidization reactions) during twin-screw extrusion. Finally, the proven possibility of realizing both oligomerization reactions by grafting i-PP with MA and a controlled preparation of the nanocomposites by reactive extrusion provide the basis for further development of the industrial preparation of high-performance engineering nanocomposite materials in one single stage.

Acknowledgments

References

1. Dubois, P.; Alexandre, M.; Hindryckx, F.; Jérôme, R. J. Macromol Sci: Rev Macromol Chem Phys 1998, C38, 511.
2. Lagalay, G. Appl Clay Sci 1999, 15, 1.
3. Ray, S. S.; Okamoto, M. Prog Polym Sci 2003, 28, 1539.
4. Okamoto, M. Rapra Rev Rep 2003, 14(7):Report 163.
5. Utracki, L. A. Clay-Containing Polymeric Nanocomposites; National Research Council Canada, Rapra Technol. 2004; Polymer News, 2005, 30, 134.
6. Kawasumi, M.; Nasegawa, H.; Kato, M.; Usuki, A. Macromolecules 1997, 30, 6333.
7. Nasegawa, H.; Kawasumi, M.; Kato, M.; Usuki, A.; Okada, A. J Appl Polym Sci 1998, 67, 87.
8. Nasegawa, H.; Okamoto, M.; Kawasumi, M.; Kato, A.; Tsukigase, A.; Usuki, A. Macromol Mater Eng 2000, 280/281, 76.
9. Nasegawa, H.; Okamoto, M.; Usuki, A. J Appl Polym Sci 2004, 93, 758.
10. Weiss, A. Angew Chem, Adv Int Ed 1963, 2, 134.
11. Alexandre, M.; Dubois, P. Mater Sci Eng 2000, 28, 1.
12. Böhning, M.; Goering, H.; Fritz, A.; Brzezinka, K.-W.; Turky, G.; Schönhals, A.; Schartel, B. Macromolecules 2005, 38, 2764.
13. Schmidt, D.; Shah, D.; Giannelis, E. P. Curr Opin Solid State Mater Sci 2002, 6, 205.
14. Tidjani, A.; Wald, O.; Pohl, M.-M.; Henschel, M. P.; Schartel, B. Polym Degrad Stab 2003, 82, 133.
15. Koo, C. M.; Kim, M. J.; Choi, S. M. N.; Kim, O.; Chung, I. J. J Appl Polym Sci 2003, 88, 1526.
16. Xu, W.; Liand, G.; Wang, W.; Tang, S.; He, P.; Pan, W.-P. J Appl Polym Sci 2003, 88, 3093.
17. Rzayev, Z. M. O.; Güner, A.; Can, H. K.; Asıcı, A. Polymer 2001, 42, 5599.
18. Zhou, W.; Dong, J. H.; Qiu, K. Y.; Wei, Y. Acta Polym Sinica 1998, 6, 730.
19. Kojima, Y.; Usuki, A.; Kawasumi, M.; Okada, A.; Fukushima, Y.; Kurauchi, T.; Kamigaito, O. J Mater Res 1993, 8, 1185.
20. Messersmith, P. B.; Giannelis, E. P. Chem Mater 1994, 6, 1719.
21. Kornmann, X.; Lindberg, H.; Berglund, L. A. Polymer 2001, 42, 1303.
22. Chen, K. H.; Yang, S. M. J Appl Polym Sci 2002, 86, 414.
23. Zhang, J.; Wilkie, C. A. Polym Degrad Stab 2003, 80, 163.
24. Tang, Y.; Hu, Y.; Wang, S. F.; Gui, Z.; Chen, Z.; Fan, W. C. Polym Degrad Stab 2002, 78, 555.
25. Gilman, J. W.; Jackson, C. J.; Morgan, A. B.; Harris, J. R.; Manias, E.; Giannelis, E. P.; Wuthenow, M.; Hilton, D.; Philips, S. H. Chem Mater 2000, 12, 1866.
26. Gilman, J. W. Appl Clay Sci 1999, 15, 31.
27. Zhu, J.; Morgan, A. B.; Lamelas, F. J.; Wilkie, C. A. Chem Mater 2001, 13, 774.
28. Yano, K.; Usuki, A.; Okada, A. J Polym Sci, Part A-1: Polym Chem 1997, 5, 2289.
29. Lan, T.; Kaviratna, P. D.; Pinnavaia, T. J. Chem Mater 1994, 6, 573.
30. Yeh, J. M.; Liou, S. J.; Lai, C. Y.; Wu, P. C.; Tsai, T. Y. Chem Mater 2001, 13, 1131.
31. Yeh, J. M.; Liou, S. J.; Lin, C. Y.; Cheng, C. Y.; Chang, Y. W.; Lee, K. B. Chem Mater 2002, 14, 154.
32. Parija, S.; Nayak, S. K.; Verma, S. K.; Tripathy, S. S. Polym Compos 2004, 25, 646.
33. Güldoğan, Y.; Eğri, S.; Rzayev, Z. M. O.; Pişkin, E. J Appl Polym Sci 2004, 92, 3675.
34. Yilmazbayhan, A.; Rzayev, Z. M. O. Abstract in European Polymer Congress, June–July, 2005, Moscow, Sec. 5, p. 131.

35. Rzayev, Z. M. O.; Yilmazbayhan, A. Abstract Book of 10th Annual Green Chemistry & Engineering Conference, June 26–30, 2006, Washington, DC; p. 44.

36. Rzayev, Z. M. O.; Yilmazbayhan, A. Abstract Book of 1st European Chemistry Congress: Symposium on Polymer Architectures—From Structure to Functional Control, August 27–31, 2006, Budapest, Hungary; p. 262.

37. Gaylord, N. G.; Mishra, M. K. J Polym Sci, Polym Lett Ed 1983, 21, 23.

38. Belofsky, H. Plastics: Product Design and Process Engineering; Hanser: Cincinnati, OH, 1985.

39. Rabek, J. F. Experimental Methods in Polymer Chemistry; Wiley: New York, 1980.

40. Kato, M.; Usuki, A.; Okada, A. J Appl Polym Sci 1997, 66, 1781.

41. Usuki, A.; Kato, M.; Okada, A.; Kurauchi, T. J Appl Polym Sci 1997, 63, 137.

42. Wouters, M. E. L.; Goossens, J. P. G.; Binsbergen, F. L. Macromolecules 2002, 35, 208.

43. Wouters, M. E. L.; Litvinov, V. M.; Goossens, J. P. G.; Binsbergen, F. L.; van Duin, M.; Dikland, H. G. Macromolecules 2003, 36, 1147.

44. Wouters, M. E. L. Ph. D. thesis, Eindhoven University of Technology, Eindhoven, The Netherlands, 2000.

45. Schmidt, U.; Zchoche, S.; Werner, C. J Appl Polym Sci 2003, 87, 1255.

46. Pawda, A. R.; Macosko, C. W.; Wolske, K. A.; Sasaki, Y. Polym Prepr (ACS Div. Polym. Chem.) 1993, 34, 842.

47. Vermeesch, I.; Groneninclx, G. J Appl Polym Sci 1994, 53, 1357.

48. Schmidt-Naake, G.; Becker, H. G.; Klak, M. Macromol Symp 2001, 163, 213.

49. Tsuwi, J.; Appelhans, D.; Zchoche, S.; Friedel, P.; Kremer, F. Macromolecules 2004, 37, 6050.

50. Rzaev, Z. M. O. Polymers and Copolymers of Maleic Anhydride; Elm: Baku, 1984.

51. Sun, C. X.; der Mee, M. A. J.; Goossens, J. G. P.; van Duin, M. Macromolecules 2006, 39, 3441.

52. Lee, W. L.; Lim, Y. T.; Park, O. O. Polym Bull 2000, 45, 191.

53. Xie, W.; Gao, Z.; Pan, W.-P.; Hunter, D.; Singh, A.; Vaia, R. Chem Mater 2001, 13, 2979.

54. Newman A. C. D. (ed.). Chemistry of Clays and Clays Minerals, Mineralogical Society Monograph No. 6; Longman Scientific & Technical: Burnt Mill, Harlow, Essex, UK, 1987.

55. Tanoue, S.; Uratcki, L. A.; Garcia-Rejon, A.; Tatibouet, J.; Cole, K. C.; Kamal, M. R. Polym Eng Sci 2004, 44, 1046.

reactions was confirmed by a comparative analysis of the thermal behavior and the MFI values of both pure i-PP and its grafted derivatives. The results have shown that an increase in grafted MA content from 0.15 to 1.22 mol% decreased the T_m value of the grafted oligomer and increased the crystallization temperature. This can be interpreted in terms of a possibility of providing nucleating centers in the crystallization process of i-PP at relatively low contents of MA units. The mechanism of formation of nanostructures was explained using the results of FTIR, DSC, and XRD analyses, as well as known structural models (intercalation and exfoliation). Relatively lower molecular weight (MFI = 61.0–35.2 g 10^{-1} min, $M_n = 3010$–3560 g mol^{-1}) of grafted copolymers, and therefore, their relatively high-swelling capacity allows them to intercalate and exfoliate easily in silicate interlayered galleries, where the anhydride-containing macromolecules interact with the surface alkyl amine groups through H-bonding and chemical interactions (amidization/imidization reactions) during twin-screw extrusion. Finally, the proven possibility of realizing both oligomerization reactions by grafting i-PP with MA and a controlled preparation of the nanocomposites by reactive extrusion provide the basis for further development of the industrial preparation of high-performance engineering nanocomposite materials in one single stage.

Acknowledgments

References

1. Dubois, P.; Alexandre, M.; Hindryckx, F.; Jérôme, R. J. Macromol Sci: Rev Macromol Chem Phys 1998, C38, 511.
2. Lagalay, G. Appl Clay Sci 1999, 15, 1.
3. Ray, S. S.; Okamoto, M. Prog Polym Sci 2003, 28, 1539.
4. Okamoto, M. Rapra Rev Rep 2003, 14(7):Report 163.
5. Utracki, L. A. Clay-Containing Polymeric Nanocomposites; National Research Council Canada, Rapra Technol. 2004; Polymer News, 2005, 30, 134.
6. Kawasumi, M.; Nasegawa, H.; Kato, M.; Usuki, A. Macromolecules 1997, 30, 6333.
7. Nasegawa, H.; Kawasumi, M.; Kato, M.; Usuki, A.; Okada, A. J Appl Polym Sci 1998, 67, 87.
8. Nasegawa, H.; Okamoto, M.; Kawasumi, M.; Kato, A.; Tsukigase, A.; Usuki, A. Macromol Mater Eng 2000, 280/281, 76.
9. Nasegawa, H.; Okamoto, M.; Usuki, A. J Appl Polym Sci 2004, 93, 758.
10. Weiss, A. Angew Chem, Adv Int Ed 1963, 2, 134.
11. Alexandre, M.; Dubois, P. Mater Sci Eng 2000, 28, 1.
12. Böhning, M.; Goering, H.; Fritz, A.; Brzezinka, K.-W.; Turky, G.; Schönhals, A.; Schartel, B. Macromolecules 2005, 38, 2764.
13. Schmidt, D.; Shah, D.; Giannelis, E. P. Curr Opin Solid State Mater Sci 2002, 6, 205.
14. Tidjani, A.; Wald, O.; Pohl, M.-M.; Henschel, M. P.; Schartel, B. Polym Degrad Stab 2003, 82, 133.
15. Koo, C. M.; Kim, M. J.; Choi, S. M. N.; Kim, O.; Chung, I. J. J Appl Polym Sci 2003, 88, 1526.
16. Xu, W.; Liand, G.; Wang, W.; Tang, S.; He, P.; Pan, W.-P. J Appl Polym Sci 2003, 88, 3093.
17. Rzayev, Z. M. O.; Güner, A.; Can, H. K.; Asıcı, A. Polymer 2001, 42, 5599.
18. Zhou, W.; Dong, J. H.; Qiu, K. Y.; Wei, Y. Acta Polym Sinica 1998, 6, 730.
19. Kojima, Y.; Usuki, A.; Kawasumi, M.; Okada, A.; Fukushima, Y.; Kurauchi, T.; Kamigaito, O. J Mater Res 1993, 8, 1185.
20. Messersmith, P. B.; Giannelis, E. P. Chem Mater 1994, 6, 1719.
21. Kornmann, X.; Lindberg, H.; Berglund, L. A. Polymer 2001, 42, 1303.
22. Chen, K. H.; Yang, S. M. J Appl Polym Sci 2002, 86, 414.
23. Zhang, J.; Wilkie, C. A. Polym Degrad Stab 2003, 80, 163.
24. Tang, Y.; Hu, Y.; Wang, S. F.; Gui, Z.; Chen, Z.; Fan, W. C. Polym Degrad Stab 2002, 78, 555.
25. Gilman, J. W.; Jackson, C. J.; Morgan, A. B.; Harris, J. R.; Manias, E.; Giannelis, E. P.; Wuthenow, M.; Hilton, D.; Philips, S. H. Chem Mater 2000, 12, 1866.
26. Gilman, J. W. Appl Clay Sci 1999, 15, 31.
27. Zhu, J.; Morgan, A. B.; Lamelas, F. J.; Wilkie, C. A. Chem Mater 2001, 13, 774.
28. Yano, K.; Usuki, A.; Okada, A. J Polym Sci, Part A-1: Polym Chem 1997, 5, 2289.
29. Lan, T.; Kaviratna, P. D.; Pinnavaia, T. J. Chem Mater 1994, 6, 573.
30. Yeh, J. M.; Liou, S. J.; Lai, C. Y.; Wu, P. C.; Tsai, T. Y. Chem Mater 2001, 13, 1131.
31. Yeh, J. M.; Liou, S. J.; Lin, C. Y.; Cheng, C. Y.; Chang, Y. W.; Lee, K. B. Chem Mater 2002, 14, 154.
32. Parija, S.; Nayak, S. K.; Verma, S. K.; Tripathy, S. S. Polym Compos 2004, 25, 646.
33. Güldoğan, Y.; Eğri, S.; Rzayev, Z. M. O.; Pişkin, E. J Appl Polym Sci 2004, 92, 3675.
34. Yilmazbayhan, A.; Rzayev, Z. M. O. Abstract in European Polymer Congress, June–July, 2005, Moscow, Sec. 5, p. 131.

35. Rzayev, Z. M. O.; Yilmazbayhan, A. Abstract Book of 10th Annual Green Chemistry & Engineering Conference, June 26–30, 2006, Washington, DC; p. 44.

36. Rzayev, Z. M. O.; Yilmazbayhan, A. Abstract Book of 1st European Chemistry Congress: Symposium on Polymer Architectures—From Structure to Functional Control, August 27–31, 2006, Budapest, Hungary; p. 262.

37. Gaylord, N. G.; Mishra, M. K. J Polym Sci, Polym Lett Ed 1983, 21, 23.

38. Belofsky, H. Plastics: Product Design and Process Engineering; Hanser: Cincinnati, OH, 1985.

39. Rabek, J. F. Experimental Methods in Polymer Chemistry; Wiley: New York, 1980.

40. Kato, M.; Usuki, A.; Okada, A. J Appl Polym Sci 1997, 66, 1781.

41. Usuki, A.; Kato, M.; Okada, A.; Kurauchi, T. J Appl Polym Sci 1997, 63, 137.

42. Wouters, M. E. L.; Goossens, J. P. G.; Binsbergen, F. L. Macromolecules 2002, 35, 208.

43. Wouters, M. E. L.; Litvinov, V. M.; Goossens, J. P. G.; Binsbergen, F. L.; van Duin, M.; Dikland, H. G. Macromolecules 2003, 36, 1147.

44. Wouters, M. E. L. Ph. D. thesis, Eindhoven University of Technology, Eindhoven, The Netherlands, 2000.

45. Schmidt, U.; Zchoche, S.; Werner, C. J Appl Polym Sci 2003, 87, 1255.

46. Pawda, A. R.; Macosko, C. W.; Wolske, K. A.; Sasaki, Y. Polym Prepr (ACS Div. Polym. Chem.) 1993, 34, 842.

47. Vermeesch, I.; Groneninclx, G. J Appl Polym Sci 1994, 53, 1357.

48. Schmidt-Naake, G.; Becker, H. G.; Klak, M. Macromol Symp 2001, 163, 213.

49. Tsuwi, J.; Appelhans, D.; Zchoche, S.; Friedel, P.; Kremer, F. Macromolecules 2004, 37, 6050.

50. Rzaev, Z. M. O. Polymers and Copolymers of Maleic Anhydride; Elm: Baku, 1984.

51. Sun, C. X.; der Mee, M. A. J.; Goossens, J. G. P.; van Duin, M. Macromolecules 2006, 39, 3441.

52. Lee, W. L.; Lim, Y. T.; Park, O. O. Polym Bull 2000, 45, 191.

53. Xie, W.; Gao, Z.; Pan, W.-P.; Hunter, D.; Singh, A.; Vaia, R. Chem Mater 2001, 13, 2979.

54. Newman A. C. D. (ed.). Chemistry of Clays and Clays Minerals, Mineralogical Society Monograph No. 6; Longman Scientific & Technical: Burnt Mill, Harlow, Essex, UK, 1987.

55. Tanoue, S.; Uratcki, L. A.; Garcia-Rejon, A.; Tatibouet, J.; Cole, K. C.; Kamal, M. R. Polym Eng Sci 2004, 44, 1046.

Ref. 2

Dynamic Viscoelasticity of Syndiotactic Poly (vinyl alcohol) Derived from Vinyl Pivalate

Ryohei Fukae[*1], *Tohei Yamamoto*[*2], *Hitoshi Masago*[*3], *Nobuhiro Kawatsuki*[*2], *Osamu Sangen*[*2], *and Mikiharu Kamachi*[*4]

[*1]Himeji Junior College, Shinzaikehoncho, Himeji 670, Japan

[*2]Faculty of Engineering, Himeji Institute of Technology, Shosha, Himeji 671-22, Japan

[*3]Aboshi Laboratory, Takiron Co.,LTD., Ibo-Gun Hyogo 671-13, Japan

[*4]Faculty of Science, Osaka University, Machikaneyama, Toyonaka 560, Japan

Abstract : Dynamic viscoelasticity of poly(vinyl alcohol) (st-PVA) with high syndiotacticity (diad-syndiotacticity > 61%), which is derived from vinyl pivalate, was investigated to compare with that of commercial atactic PVA (at-PVA, diad-syndiotacticity = 54%). Cast films of at-PVA with D_p of 1,800 (at-L), st-PVA with D_p of 1,700 (st-L) and st-PVA with D_p of 12,500 (st-H) were prepared and annealed to provide for the desired crystallinity. at-L and st-L show four damping dispersions, *i.e.*, β_a, α_a, β_c, and α_c, on their tanδ curves. β_a and α_a relaxations are mechanical damping of amorphous regions, whereas β_c and α_c are those of crystal regions. Dynamic storage modulus E' of (st-L)s increased with increasing crystallinities and could exceed E' of (at-L)s at temperatures beyond α_a dispersion region. In particular, st-L having a crystallinity more than 50% holds E' of 10^9 Pa order of magnitude at temperatures above 100℃. The higher value of E'' throughout the temperature ranges of glass transition-, rubbery plateau- and crystal relaxation-regions were observed when st-PVA films were drawn by 4 time the length at 180℃. In this case, tanδ_{max} (T_g) of st-PVA shifted to a higher temperature than that of at-PVA. There are no marked differences in the changes of E' and tanδ between st-L and st-H. The effects by water swelling against amorphous region, sizes of crystallites for at-PVA and st-PVA on the dynamic viscoelastic behaviors were discussed.

1. Introduction

The present report deals with the studies on the effect of stereoregularity on the dynamic viscoelasticities of poly(vinyl alcohol) (PVA), which is derived from vinyl pivalate(VP). Temperature dependencies of relaxation behaviors for solvent-cast films of PVA are discussed associated with the changes in crystallinity and tacticity.

PVA having a high molecular weight and a high degree of syndiotacticity can be prepared from poly(vinyl pivalate) (PVP) which is synthesized by photo-emulsion polymerization of VP at low temperature without a catalyst[1]. Trimethyl acetyl

substituents of PVP can be preferentially oriented in the highly syndiotactic configuration on the basis of their steric effect, and the steric effect is favored over other poly(vinyl ester)s. PVA derived from PVP is accordingly given a high syndiotacticity and its physical properties are characterized by the strong intermolecular forces owing to stereoregulated OH side groups.

Predominant mechanical properties which arise from the characteristic intermolecular force of syndiotactic PVA have been studied by many investigators. In the studies on a high syndiotactic PVA derived from poly(vinyl trifluoroacetate) (PVTFA), much instructive information with regard to the

stereoregularity have been given by Yamaura *et al.*[2].

Compared with those studies, the stereoregularity of PVA derived from PVP in our laboratory gave more satisfactory results. PVA with high degree of polymerization could be synthesized and its syndiotacticity was higher than that in PVA derived from PVTFA (PVApvtfa) under the nearly same polymerization conditions. The PVA having high molecular weight and high syndiotacticity can be expected to be utilized in a wide variety of materials with new functionality and high performance.

The investigations of the viscoelastic behavior are considered important to make clear the functions of molecular chain with stereoregulated OH groups in amorphous region. Nagura *et al.* reported of the viscoelastic behavior of PVApvtfa with high syndiotacticity[3]. However, there are no discussions with molecular thermal motion using the samples having the same crystallinities, in other word, the same amounts of amorphous regions. The changes in viscoelasticity of PVA must be influenced by the difference in crystallinity, in analogy with that in the stereoregularity and it is preferable to discuss the viscoelastic behaviors using the samples with the same crystallinity.

In the present work, the viscoelastic behaviors of PVA derived from PVP were studied, especially paying attentions to the changes in crystallinity and in the degree of polymerization. Effective role of syndiotacticity affecting the physical properties is dicussed further.

2. Experimental

2.1 Samples

Degrees of polymerization (D_p), diad-syndio-tacticities and degrees of saponification for PVA used in the present work are summarized in Table 1. The commercially available atactic PVA with syndiotacticity of 54% is called at-L, and PVA with syndiotacticity of 61% is called st-L. PVA with syndiotacticity of 63% and high degree of polymerization is called st-H. st-L and st-H were prepared from PVP in our laboratory. Polymerization of VP and saponification of the resulting PVP were done using the method previously reported by us[4].

D_p of PVA was determined from the intrinsic

Table 1 PVA Samples Used in the Present Work

PVA samples	D_p[a]	Diad-syndio tacticity[b]/%	Degree of saponification[b]/%
st-L[c]	1,690	61.2	>99.9
st-H[d]	12,500	62.8	>99.9
at-L[e]	1,750	53.9	>99.9

[a] Estimated from intrinsic viscosity of acetylated PVA.
[b] Determined from ^{1}H NMR spectrum.
[c] Derived from PVP being polymerized in MeOH solution at 60℃.
[d] Derived from PVP being photo-emulsion polymerized at 0℃.
[e] Commercial PVA, which is derived from PVAc.

viscosity of acetylated PVA in benzene at 30℃. The degrees of syndiotacticity and saponification were determined from the ^{1}H NMR spectrum of PVA[5].

2.2 Casting

PVA films used for investigation are listed in Table 2. at-L and st-L films were prepared from their aqueous solution by casting, and after drying *in vacuo* at 50℃. The number in parenthesis added to the ending of abbreviation, *e.g.*(1) of at-L(1) represents the difference in annealing condition and crystallinity of sample film. Both at-L(1) and the st-L(1) could be provided for the

Table 2 Abbreviations, Annealing Conditions and Physical Properties for PVAs

Film samples	Heat-treatment[a] /℃	X_c[b] /%	T_m[c] /℃	T_g[d] /℃	Viscoelasticity[e] tan$\delta \times 10^2$ 25℃	180℃	$E' \times 10^{-8}$/Pa 25℃	180℃
at-L(1)	——	20	——	45	23.2	18.5	27.6	1.3
at-L(2)	100.	28	——	70	6.2	17.0	74.0	1.3
at-L(3)	200	48	232	70	5.1	11.2	71.3	3.3
st-L(1)	——	20	——	56	6.8	16.8	53.5	2.4
st-L(2)	140	29	——	67	6.1	17.6	69.7	2.3
st-L(3)	200	52	243	66	5.6	9.5	68.0	5.8
st-L(4)[f]	200	57	——	68	4.7	18.4	57.2	4.6
at-L-W[g]	200	48	——	39	26.9	16.9	23.9	1.8
at-L-D[h]	180	51	——	50	11.1	10.4	174	10.6
st-L-D[h]	180	48	——	75	6.5	10.2	255	18.3
st-H[f]	200	53	248	68	4.6	18.9	60.5	4.4

[a] Heat-treatment was carried out for 15min in inert atmosphere.
[b] Crystallinity. [c] Crystal melting determined by DSC [d] Peak temperature at tanδ_{max}.
[e] tanδ, loss tangent : E', storage modulus. [f] Film casted from HFP solution.
[g] Film containing 20% of H_2O. [h] Film was drawn to 400% of original length at 180℃.

crystallinity of about 20% only under such a given film-forming condition. at-L(2), at-L(3), st-L(2) and st-L(3) were prepared by further annealing of at-L(1) and st-L(1) to have different crystallinities.

st-H and st-L(4) films were cast from their 1,1,1,3,3,3-hexafluoro-2-propanol (HFP) solutions. Poly (vinyl acetate) (PVAc) films were cast from their THF solutions.

2.3 Acetylation of PVA

One gram of PVA, 2ml of pyridine, 20ml of acetic anhydride and 20ml of acetic acid were placed in a three-necked flask and reacted at 100°C for 72h with stirring in inert atmosphere. The PVAc obtained was reprecipitated from methanol and water, and dried *in vacuo* at 60°C.

2.4 Determination of Crystallinity

Crystallinities of film samples were estimated from their densities using the assumption that the densities of a fully amorphous sample and a fully crystalline sample of PVA are 1.269 and 1.345 g/cm³, respectively [6]. The density was measured at 25°C by a floating method in light liquid paraffin-carbon tetrachloride mixed solution.

2.5 Determination of Crystal Size

Apparent crystal size was estimated by calculating the width of half the maximum intensity of the X-ray diffraction peak on the 101 reflection by the use of Scherrer's equation[7].

2.6 Dynamic Viscoelasticity

Dynamic storage modulus E', loss modulus E'' and loss tangent (tanδ) were measured at 110Hz with a heating rate of 2°C/min from −130°C to 230°C using a dynamic viscoelastic spectrometer DVE-V4 (Rheology Engineering Co., Ltd.).

2.7 Melting Point

Determination of crystal melting points was carried out by using a differential scanning calorimeter DSC 8230 (Rigaku Denki Co., Ltd.). The heating rate was 10°C/min.

2.8 Determination of Degree of Swelling

Degree of swelling was determined by dipping the film samples in water at the prescribed temperature and was defined by the following formula : Degree of swelling = (weight of swollen films − weight of dried films after swelling) / (weight of dried films after swelling).

3. Results and Discussion

3.1 Dynamic Mechanical Properties of at-L and st-L

Changes in E' and E'' of at-L(1) and st-L(1) with an increase in temperature are shown in Figure 1, and changes in tanδ are shown in Figure 2. Crystal melting (T_m), glass transition temperature (T_g, peak temperature of tanδ_{max} in α_a dispersion) and viscoelasitic data obtained in the present work are summarized in Table 2.

Four dispersion peaks can be confirmed in Figure 2. They are assigned to β_a, α_a, β_c, and α_c in the order from the low temperature region. β_c and α_c of crystal relaxation appear to be one dispersion peak by overlapping of two dispersions in Figure 2. Here, we notice that separated dispersions of β_c and α_c can be distinctly observed in crystal relaxation region when at-L and st-L have high crystallinities as will be described below.

β_a dispersion is a maximum dispersion which is observed at −50°C for at-L(1). It is assigned to the skeletal chain motions. This local twisting mode of skeletal chain is caused by defects in the frozen glassy regions or the crystalline regions[8]. β_a dispersion for
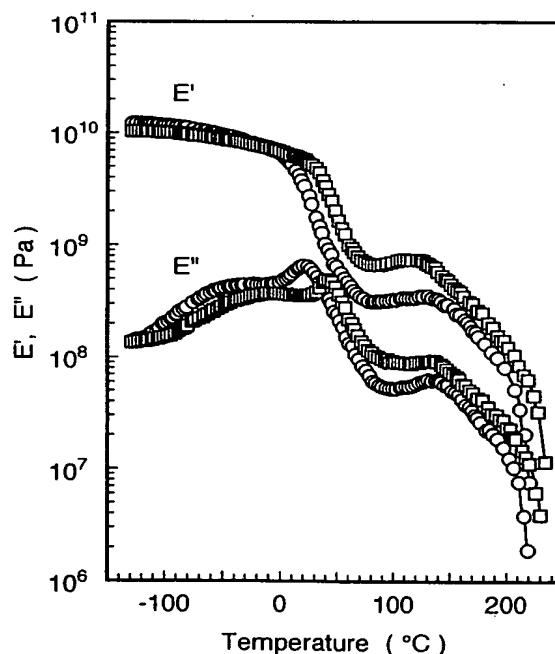

Fig. 1 Plots of dynamic storage modulus E' and loss modulus E'' vs. temperature for non-annealed PVA films: O, at-L(1); □, st-L(1).
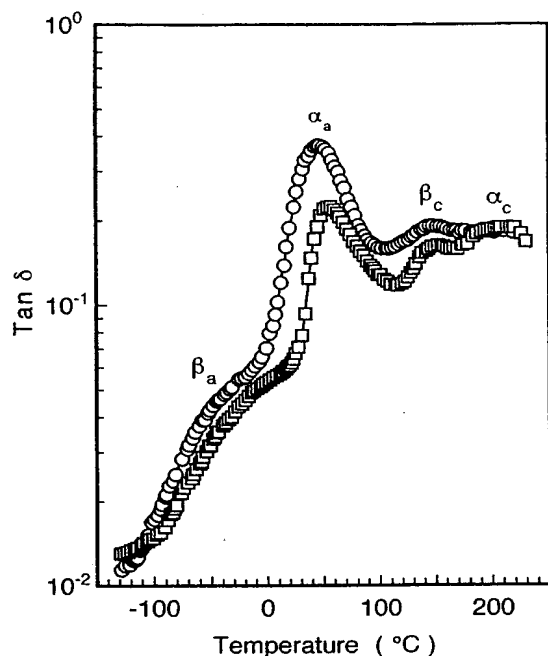
Fig. 2 Plots of tan δ vs. temperature for non-annealed PVA films: O, at-L(1); □, st-L(1).

Fig. 3 Plots of dynamic storage modulus E' and tan δ vs. temperature for at-L film containing water: □, at-L-W; O, at-L(3).

st-L(1) is observed at $-30°C$.

On the other hand, α_a dispersions is observed at temperatures near 45°C in at-L(1) and that in st-L(1) near 56°C. It is attributable to the main glass transition, *i.e.*, the micro-Brownian motions of skeletal chains in the amorphous region.

Though the crystallinities of at-L(1) and st-L(1) in Figure 2 are approximately even, α_a and β_a dispersions in st-L(1) are observed in a somewhat higher temperature region than those in at-L(1). In the present work, the samples were sufficiently dried at 60°C *in vacuo* or annealed above 100°C *in vacuo*. However, it was very difficult to satisfactorily remove residual water in the sample. A plasticizing effect of water remaining in the film may appear to causes a lowering of T_g. The effect may be responsible for weakening of intermolecular forces. The reason seems to be that β_a dispersion of at-L(1) was observed at temperatures below $-20°C$.

Figure 3 shows the viscoelastic behaviors of at-L-W. at-L-W refers to at-L(3) containing 20% water by weight. Intensity of the tan δ peak of at-L-W within α_a dispersion region increases remarkably and the peak temperature shifts toward the low temperature region as the water content increases. At the same time, the center of β_a dispersion of at-L-W shifts to the low
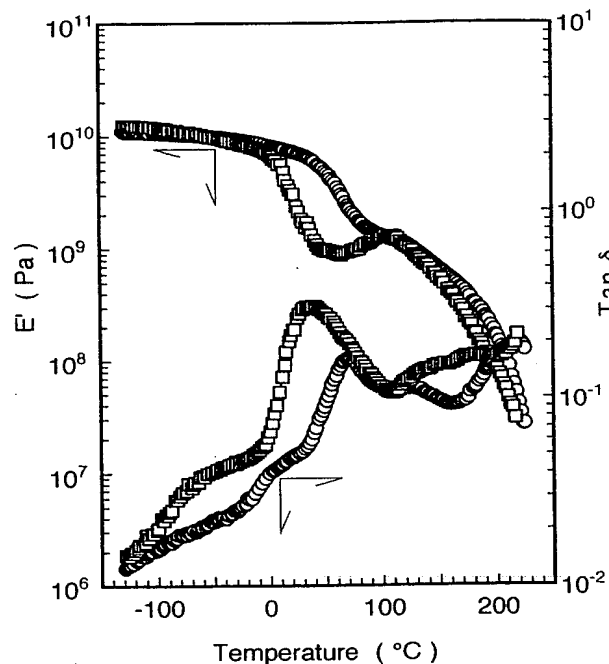
temperature region for several factors. As the remaining water is evaporated from amorphous region at temperatures above 100°C, changes of the plotted E' values in at-L-W return to the values of the original E' curve of the at-L(3). β_c dispersion, then, clearly develops and tends to overlap with α_c dispersion.

Increase of crystallinity tends to decrease the peak intensity of β_a dispersion and make a shift of the dispersion peak toward the high temperature region as shown in Figure 4 and 5. As a result, β_a dispersion is observed at a temperature near 20°C, known usually as the β_a dispersion region of PVA, and sometimes observed as a discernible shoulder at α_a dispersion.

Center of the β_c dispersion peak of at-L(1) appears in 140°C and there can be observed an incomplete separation between β_c- and α_c-dispersion when at-L(1) has low crystallinity. This would be likely due to the degeneration of α_c dispersion toward the high temperature side of β_c dispersion peak and results in broadening of dispersion peak consequently. As the crystallinity increases, peak separation of crystal relaxation in at-L(3) into two dispersions becomes clear and they can be observed at 120°C (β_c dispersion) and at 200°C (α_c dispersion), respectively, as shown in Figure 4. The β_c dispersion is assigned to the local motions by
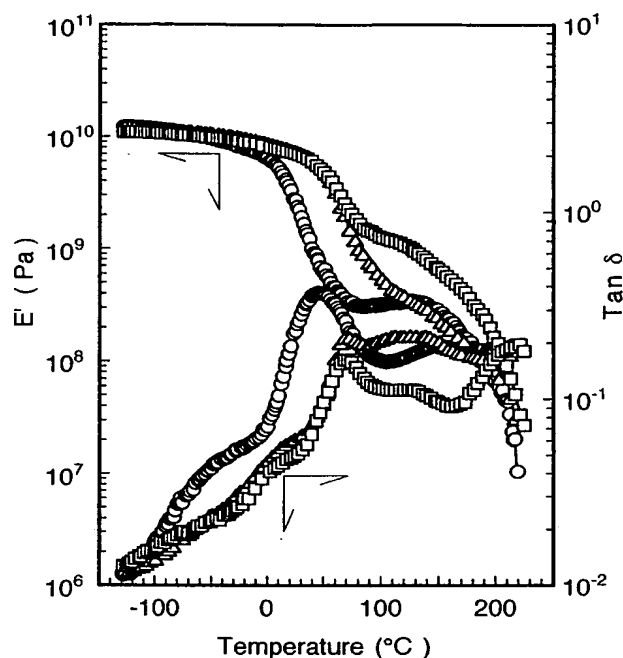
Fig. 4   Plots of dynamic storage modulus E' and tanδ
vs. temperature for at-L films with various
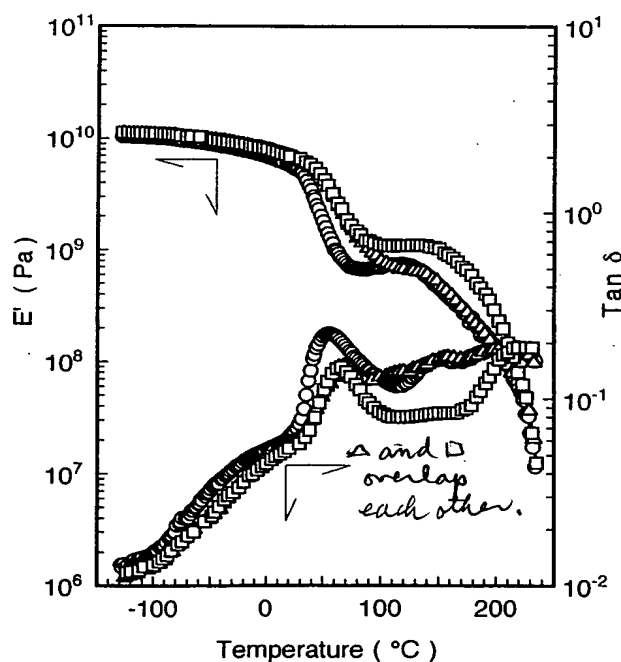crystallinities: ○, at-L(1); △, at-L(2); □, at-L
(3).

Fig. 5   Plots of dynamic storage modulus E' and tanδ
vs. temperature for st-L films with various
crystallinities: ○, st-L(1); △, st-L(2); □, st-L
(3).

the defects of molecular chain in crystals. It results

from lowering of intermolecular forces[8,9]. The
lowering of intermolecular forces, in this case, takes
place with the thermal expansion of PVA crystals.
Whereas, α_c dispersion is assigned to thermal motions
of the molecular chain along c-axis in crystal region.

3.2   Viscoelastic Behaviors of (at-L)s and (st-L)s with Different Crystallinities

Viscoelastic behaviors of (at-L)s and (st-L)s of
differing crystallinities are shown in Figure 4 and 5.

Peak intensities of the tanδ in at-L(2), at-L(3), st-L
(2) and st-L(3) lower with increases in their
crystallinities, and their tanδ peaks shift to high
temperature regions. Though dispersion behaviors of
at-L(1) or st-L(1) having low crystallinity vary with
changes in annealing conditions, comparatively little
changes in at-L(2) or st-L(2) with crystallinity of near
30% were observed, and similar tendency is seen in the
at-L(3) and st-L(3). Peaks of α_a dispersion in at-L(2)
and at-L(3) come to couple with β_c dispersion peaks and
the coupled peaks can be distinctly detected in the
crystal relaxation region. While the intensities in those
of st-L(2) and st-L(3) are rather low, it appears natural
that β_c dispersion is absorbed by α_c dispersion.

E' of (st-L)s increases as their crystallinities increase
and exceed E' of (at-L)s at the temperature range
beyond α_a dispersion region. The formation of the
plateau region on the E' curve in (st-L)s beyond the α_a
dispersion region suggests the contributions of strong
intermolecular forces due to the pseudo-crosslinking
effect of crystallites. This contribution is due to
syndiotactic regulation. In particular, st-L having a
crystallinity more than 50% keeps E' of 10^9 Pa order of
magnitude above 100℃. The β_c dispersion peak
disappears and degenerates with the α_c relaxation
peak. The α_c dispersion peak can be confirmed clearly
at about 200℃. The disappearance of the β_c dispersion
peak may be due to the thickening and completion of
crystallites in st-L(3). An annealing temperature above
200℃ for st-L(3) would allow a regeneration of crystal
regions.

Relations between annealing temperatures and
crystallinities for at-L and st-L cast films heat-treated
in inert atmosphere are shown in Figure 6. Different
plots are shown for variations in apparent grain sizes
of crystallites against annealing temperatures. These
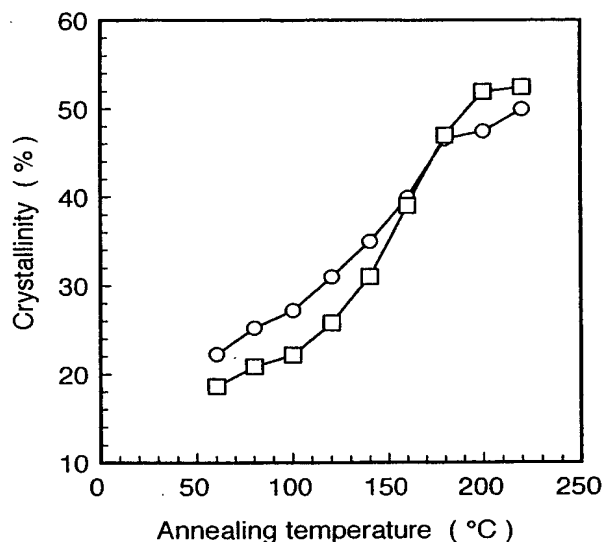are shown in Figure 7. At the same annealing

Fig. 6 Plots of crystallinities *vs.* annealing temperatures for PVA films: O, at-L; □, st-L: Annealings were carried out for 30 min under an inert atmosphere: Crystallinity was estimated by means of density method.
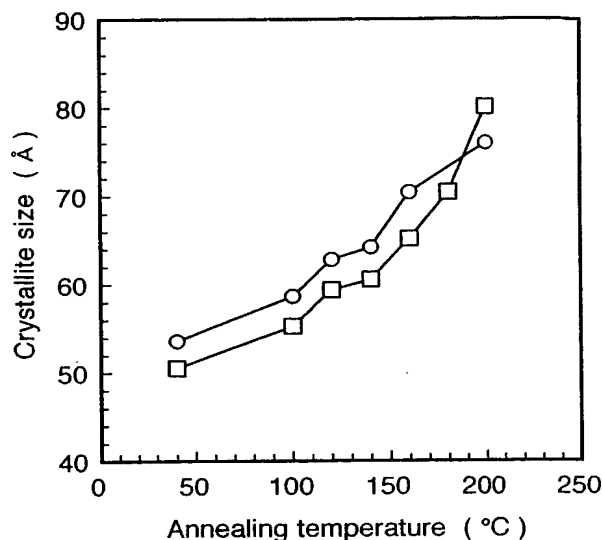
Fig. 7 Plots of crystallite sizes *vs.* annealing temperatures for PVA films: O, at-L; □, st-L: Annealings were carried out for 30 min under an inert atmosphere: Crystallite sizes were estimated by calculating the width of half the maximum intensity of 101 peak using Scherrer's equation.

temperature below 180℃, the crystallinities of (st-L)s are lower than those of (at-L)s. Glass transition of amorphous PVA is observed at about 50℃ to 80℃ as above mentioned. Therefore, the fact that the crystallinities of (st-L)s does not reach the same values as those of (at-L)s until about 180℃, may be attributable to the effect of strong intermolecular forces brought by the syndiotactic sequences in (st-L)s. The intermolecular forces described above restrict the thermal motions of amorphous chains to hinder further crystal growth by chain reordering below 180℃.

By annealing at high temperatures above 180℃, however, the crystallinities and apparent crystal sizes of (st-L)s become larger than those of (at-L)s. The melting point of st-L(3) annealed at 200℃ is 243℃ and is higher than 232℃ of the corresponding at-L(3) as shown in Table 2. This seems to be associated with the differences of changes in E', E'' and $\tan\delta$ at β_c dispersion region between at-L and st-L, and in the case of st-L, it would be expected to facilitate the rearrangement and ordering of molecular chains by annealing above 180℃.

3.3 Changes in Viscoelastic Behaviors of at-L and st-L by Draw- and Heat-treatment

Changes in E' and $\tan\delta$ with temperature for at-L-D

and st-L-D film samples, which are prepared by draw- and heat-treatment of at-L(1) and st-L(1), are shown in Figure 8 and 9, respectively. Draw- and heat-treatment were carried out by stretching the film sample four times the original length at 180℃ in inert atmosphere. Drawing significantly promotes the molecular orientation and crystallization of st-L(1). The peak of α_a dispersion in st-L-D is observed at a higher temperature by 35℃ than that in st-L(1) and the intensity of dispersion is lower than that in st-L(1).

E' of st-L-D is larger by several times than those of st-L(1). The extent of changes from st-L(1) to st-L-D is more obvious than that from at-L(1) to at-L-D. Marked change in T_g is observed by draw- and heat-treatment for st-L(1) compared to at-L(1) having the same crystallinity. Decrease in dispersion intensity and a significant shift of $\tan\delta_{max}$ for st-L suggest that thermal molecular motion in the amorphous region is largely influenced by junction points formed by syndio-regulated OH groups as is described in the following section.
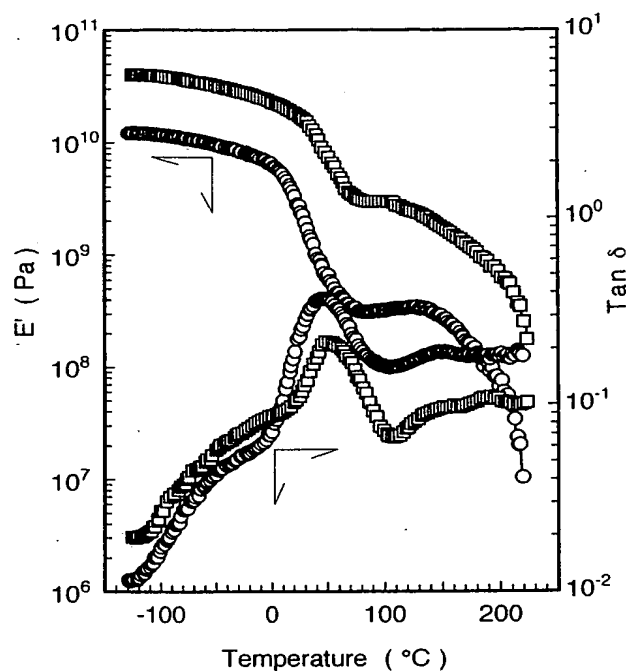
Fig. 8   Plots of dynamic storage modulus E' and tan δ vs. temperature for the draw- and heat-treated at-L film: □, at-L-D; O, at-L(1).

Fig. 9   Plots of dynamic storage modulus E' and tan δ vs. temperature for the draw- and heat-treated st-L film: □, st-L-D; O, st-L(1).

3.4   Degree of Swelling of at-L and st-L

Figure 10 shows changes in the degree of swelling with an increase in temperature when the films of (at-L) s and (st-L)s are dipped in water.

The degree of swelling of (at-L)s is higher than those of (st-L)s and there are marked differences in the degree of swelling between (at-L)s and (st-L)s having the nearly same crystallinity. The degree of swelling in (at-L)s is highly dependent on their crystallinities. On the contrary, slight difference due to crystallinity was observed in the case of (st-L)s. (st-L)s are not susceptible to swelling with water. Even st-L (Xc=34%) having the lowest crystallinity among st-L homologs is difficult to be swollen.

The degrees of swelling of (at-L)s and (st-L)s begin to increase at each definite temperature region, i.e., (at-L)s begin to increase at 40℃ and (st-L)s begin to increase at 60℃. However, these increases are not dependent on the crystallinity. Difference of the degree of swelling among the PVA homologs with the same crystallinity is attributable not to an amount of amorphous region but rather is due to the ability of hydration by the molecular chain. Sakurada et al., elucidated that swelling in water for PVA having low
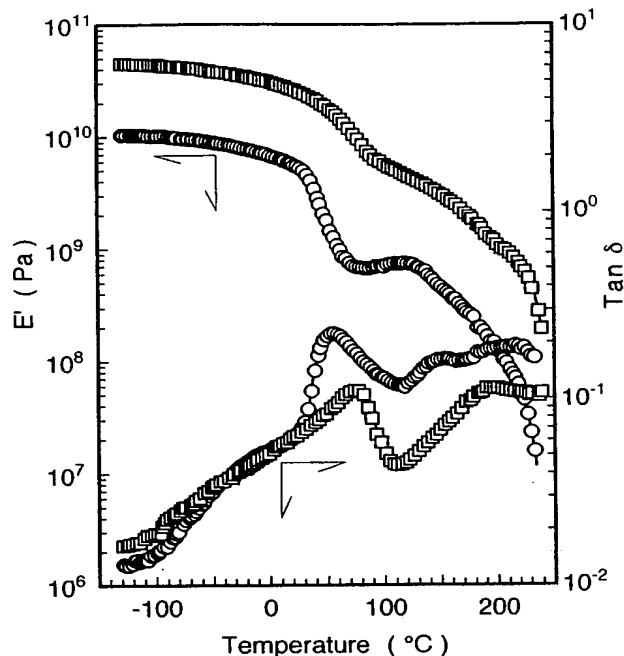
crystallinity is markedly governed by the average chain length in the amorphous region[6]. We suppose that tightly formed hydrogen bonds by a number of junction points in (st-L)s make difficult to disaggregate by H_2O molecules.
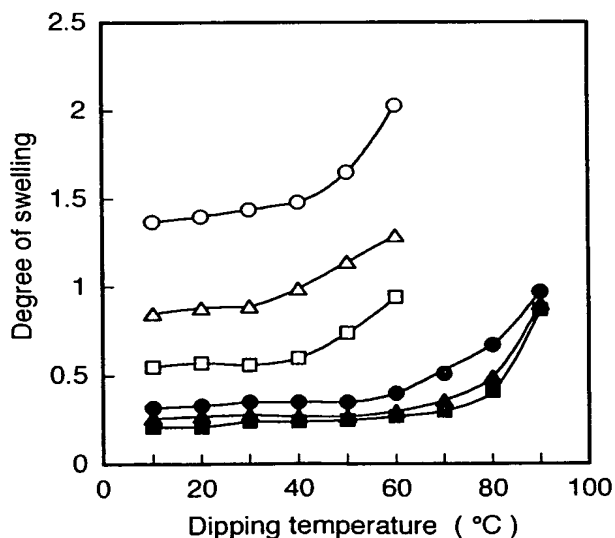

Fig.10   Swelling behaviors of PVA films for water: O, at-L(crystallinity, (Xc) =41%); △, at-L(Xc= 44%); □, at-L(Xc=49%); ●, st-L(Xc=34%); ▲, st-L(Xc=40%); ■, st-L(Xc=47%).

3.5 Comparison of Viscoelastic Behaviors of st-H with st-L

Effects of degrees of polymerization on visco-elasticities for st-L(4) (Xc=57%) and st-H (Xc=53%) were tested. Temperature dependencies of tanδ and E' are shown in Figure 11. High syndiotactic st-H with syndiotacticity of 63% is difficult to dissolve in water, therefore, its film is cast from HFP solution.

As shown in Figure 11, there are no significant differences in both the E' curves and tanδ curves between st-L and st-H. Difference in degree of polymerization nearly shows no influence on viscoelastic behaviors for PVA derived from PVP (st-PVA) when its syndiotacticity and crystallinity are very high. We reported previously that fiber property of st-PVA having a degree of polymerization of about 2,000 would be comparable to that of st-PVA with high degree of polymerization above 5,000[10].

3.6 Thermal Motions of Amorphous Chain in PVA

Glass transition temperatures (T_g.s) of at-PVAc and st-PVAc, which were prepared from at-L and st-L by acetylation, were determined by viscoelastic measurement. The results obtained are shown in Figure 12.

T_g.s of at-PVAc and st-PVAc are identical with each other. Effects of syndiotactic acetyl substituents on the thermal motion of skeletal chains are scarcely observed in tanδ behaviors. This suggests that tacticity effects by substituents on the rotating motion of a skeletal chain for vinyl polymers may be small, comparing the steric effects by bulkiness of substituents. There are appreciable differences in peak temperatures of tanδs among PVAs having different tacticities, even if they have the same crystallinity. As the hydroxyl substituent in PVA is smaller in volume than that of the acetyl group, it is sure that polarity of the hydroxyl substituents in PVAs affects their micro-Brownian motions.

It is reasonable to consider that, in the case of PVA, the intermolecular forces by stereoregulated hydroxyl substituents should have a strong effect upon the rotating of skeletal chains. The tanδ_{max} of st-PVA must be observed at a higher temperature than that of at-PVA because the appreciable intermolecular forces caused by syndiotactic regulation serves to increase the physical properties for st-PVA. However, the peak of tanδ_{max} in highly syndiotactic PVA often appears at a
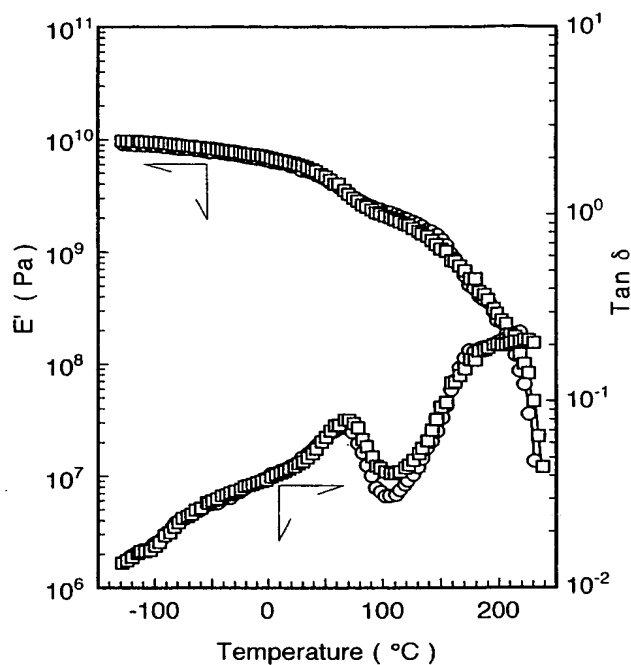

Fig.11 Plots of dynamic storage modulus E' and tanδ vs. temperature for PVA films: O, st-L(4); □, st-H.

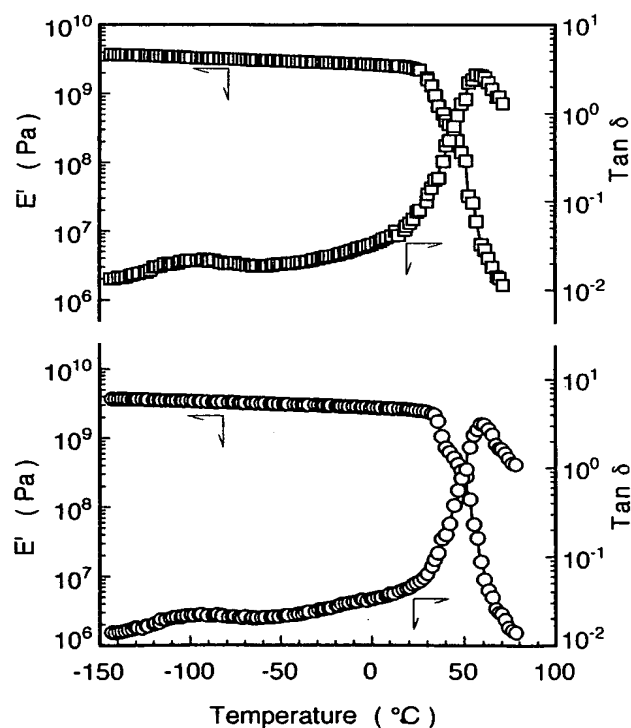**Fig.12** Plots of dynamic storage modulus E' and tanδ vs. temperature for poly(vinyl acetate)films: O, at-PVAc; □, st-PVAc.

lower temperature than that of atactic PVA. The inexplicable variation in T_g among PVAs suggests that the thermal motion of PVA molecular chain is influenced not only by intermolecular forces but the complexity arising from the difference of molecular chain length in the amorphous region, and changes in size and dispersion of crystallites.

Acknowledgement

References

1. T. Yamamoto, S. Yoda, O. Sangen, R. Fukae, and M. Kamachi, *Polym. J.,* **21,** 1053 (1989).

2. For example, K. Yamaura, *Kobunshi Kako,* **41,** 73 (1992).

3. M. Nagura, S. Matsuzawa, K. Yamaura, and H. Ishikawa, *Polymer Communications,* **24,** 250 (1983).

4. T. Yamamoto, S. Yoda, H. Takase, T. Saso, O. Sangen, R. Fukae, M. Kamachi, and T. Sato, *Polym. J.,* **23,** 185 (1991).

5. T. Moritani, I. Kuruma, K. Shibatani, and Y. Fujiwara, *Macromolecules,* **5,** 577 (1972).

6. I. Sakurada, T. Nukushina, and Y. Sone, *Kobunshi Kagaku,* **12,** 506 (1955).

7. T. Hayasaki, M. Shibayama, S. Sakurai, S. Nomura, H. Fujiwara, and S. Suehiro, *Sen-i Gakkaishi,* **47,** 75 (1991).

8. A. Nagai and M. Takayanagi, *Kogyo Kagaku Zasshi,* **68,** 836 (1965).

9. K. Shiragashi, K. Ishikawa, and K. Miyasaka, *Kobunshi Kagaku,* **21,** 588 (1964).

10. R. Fukae, T. Yamamoto, Y. Imori, O. Sangen, and M. Kamachi, *Sen-i Gakkaishi,* **52,** 434 (1996).